

EFFECT OF STACKING FAULT ENERGY ON TEXTURE
TRANSITION IN ALPHA BRASSES

by

Carlos G. Valenzuela

A Thesis Submitted to the Faculty of the
DEPARTMENT OF METALLURGICAL ENGINEERING
In Partial Fulfillment of the Requirements
For the Degree of
MASTER OF SCIENCE

In the Graduate College
THE UNIVERSITY OF ARIZONA

1965

STATEMENT OF AUTHOR

This thesis has been submitted in partial fulfillment of requirements for an advanced degree at The University of Arizona and is deposited in the University Library to be made available to borrowers under rules of the Library.

Brief quotations from this thesis are allowable without special permission, provided that accurate acknowledgment of source is made. Requests for permission for extended quotation from or reproduction of this manuscript in whole or in part may be granted by the head of the major department or the Dean of the Graduate College when in his judgment the proposed use of the material is in the interests of scholarship. In all other instances, however, permission must be obtained from the author.

SIGNED: _____

Carlos Velasco

APPROVAL BY THESIS DIRECTOR

This thesis has been approved on the date shown below:

L. J. Demer

L. J. Demer
Professor of

Metallurgical Engineering

5/6/65
Date

ACKNOWLEDGMENT

The author is especially indebted to his advisor, Dr. L. J. Demer, for his interest and helpful suggestions throughout the investigation.

Special thanks are also due to A. W. Stephens who helped greatly in the texture study.

The high purity copper donated by American Smelting and Refining Company is gratefully acknowledged.

The assistance of my sister, Sylvia, in plotting of pole figures and typing of the rough draft of the manuscript is also appreciated.

TABLE OF CONTENTS

	Page
LIST OF FIGURES.....	iv
LIST OF SKETCHES.....	viii
LIST OF TABLES.....	ix
ABSTRACT.....	x
I INTRODUCTION.....	1
II THEORETICAL BACKGROUND.....	5
2.1 Rolling Textures in FCC Metals.....	5
2.2 Stacking Faults.....	12
2.3 Dependence of Texture on Stacking Fault Energy.....	23
2.4 Effect of Solute Additions on Interfacial Energy.....	25
III OBJECTIVES.....	28
IV MATERIALS AND PROCEDURE.....	29
V RESULTS.....	33
5.1 Twin Boundary Energies.....	33
5.2 Rolling Textures.....	34
5.3 Dependence of Texture on Stacking Fault Energy.....	36
VI DISCUSSION.....	38
6.1 Twin Boundary Energies.....	38
6.2 Effect of Solute Addition on Twin Boundary Energy.....	48
6.3 Twin Boundary Energy vs Stacking Fault Energy.....	51
6.4 Texture Intensity Ratios.....	58
6.5 Effect of Stacking Fault Energy on Rolling Texture.....	59

	Page
VII SUMMARY.....	64
VIII CONCLUSIONS.....	66
REFERENCES.....	68
APPENDIX A.....	91
APPENDIX B.....	97

LIST OF FIGURES

Figure		Page
1	Ball model of (a) splitting of total dislocation into partials; (b), (c) resulting fault.....	74
2	Distribution of values of twin/grain boundary energy for pure copper and 1.03 w/o zinc in brass.....	78
3	Distribution of values of twin/grain boundary energy for 2.60 w/o zinc and 5.30 w/o zinc in brass.....	79
4	Distribution of values of twin/grain boundary energy for 6.85 w/o zinc and 12.88 w/o zinc in brass.....	80
5	Variation of mean and range of confidence with number of values of twin/grain boundary energy measured.....	81
6	Twin and grain boundary energies for Cu-Zn alloys.....	82
7	{111} pole figures of high purity copper and brass rolled 98.3%. Weight percent zinc in brass as indicated. □{110} <112> Δ {531} <001>.....	83
8	{111} pole figures of high purity brass rolled 98.3%. Weight percent zinc in brass as indicated. □{110} <112> Δ {531} <001>.....	84
9	{111} pole figures of brasses rolled 96%. Weight percent zinc in brass as indicated. (After Merlini and Beck, 1955).....	85
10	Variation of texture intensity ratio with weight percent zinc in brass.....	86

Figure		Page
11	Partial $\{111\}$ pole figure scan of 99.99% copper rolled 76%.....	87
12	Partial $\{111\}$ pole figure scan of 99.999% copper rolled 98.3%.....	88
13	Apparent stacking fault energies for copper- zinc alloys.....	89
14	Variation of texture intensity ratio with stacking fault energy.....	90

LIST OF SKETCHES

Sketch		Page
1	Surface tension and partial dislocation repulsion vs distance of separation of partials.....	13
2	Burger's vector relations on $\{111\}$ plane of FCC crystal.....	16
3	Dislocation node containing faulted areas.....	19
4	Twinned Crystal.....	21
5	Mechanical analogy of twin surface energy.....	21
6	Stacking fault with constriction.....	23
7	Specimen mount for electropolishing.....	32
8	Formation of an annealing twin.....	42
9	Some observations of twinned grains.....	43
10	Schematic plot of Fermi energy vs $\{111\}$ d-spacing across a stacking fault.....	57

LIST OF TABLES

Table		Page
I	Detailed chemical analysis of high purity copper and zinc.....	71
II	Twin Boundary energy data.....	72
III	Texture parameters and stacking fault energies.....	73

ABSTRACT

The method of obtaining twin boundary energies by measurement of dihedral angles at twin-grain junctions can be extended to alloys. Twin boundary energies can be used as a guide to stacking fault energies. This method is more reliable for estimating stacking fault energy in metals with higher stacking fault energy than the method involving measurements of radii of dislocation nodes due to the limit of resolution of the electron microscope.

Stacking fault energy in low zinc brasses does not decrease in a simple exponential manner with increasing zinc as is usually indicated by extrapolated values from brasses of higher zinc content. This energy actually decreases rapidly for the first additions of zinc up to about 1 weight percent after which the rate of decrease is lower.

The copper-to-brass texture transition is shown to depend on a decrease in stacking fault energy.

C
A
B
C
B
A
C

Annealing-twin fault

Stacking fault energy may be measured by essentially three methods: (a) electron microscope observation of dislocation nodes, (b) x-ray measurements of peak shifts, and (c) measurement of coherent-annealing-twin dihedral angles.

Measurement of dislocation nodes is limited to alloys with a minimum of about 10 percent zinc in brasses due to limits of resolution of the electron microscope (Thomas, 1963). The x-ray method yields fairly good results for the frequency of stacking faults but it is difficult to obtain stacking fault energies from this frequency because values of dislocation density are required. At present, dislocation densities can only be estimated in metals because of the high density, about 10^{11} dislocations/cm² for cold-worked metal. The method involving measurement of annealing-twin dihedral angles seems promising because it yields the ratio of twin boundary energy to grain boundary energy. The stacking fault energy is assumed to be twice the twin boundary energy (Read, 1953). Although this method has been used only for pure metals (Fullman, 1950; Inman and Khan, 1961;

Bolling and Winegard, 1958), it may be possible to extend this method to alloys.

Addition of a solute to a pure FCC metal lowers its stacking fault energy (Howie and Swann, 1961, for instance). Lowering the stacking fault energy has been suggested as a means of changing the deformation mode through the change in cross-slip phenomena (Seeger, 1959; Thornton, Mitchell, and Hirsch, 1962). Since a change in cross slip would change lattice rotations during plastic deformation, it would be expected that this change could be shown by a change of preferred orientation, or texture, of the material.

Several papers have been written on the existence and types of preferred orientations, or textures, in metals and alloys (Hu and Goodman, 1963; Merlini and Beck, 1955; Hu, Sperry, and Beck, 1952; Dillamore and Roberts, 1964). Because of the pronounced anisotropy produced by some textures, a practical importance exists in understanding the fundamental causes of textures so that eventually desired formation or suppression of these can be exercised.

Mechanisms operative in the formation or alteration of textures are somewhat elusive because of the difficulty of separating the experimental variables that contribute to the formation of these textures. However, it is known that textures are the result of processing

the original ingots, alloying additions, plus methods and temperature of deformations. In the processing of the original ingots, the type and degree of texture is a function of the casting and subsequent heat-treating process.

Alloying additions seem to cause a change in texture from the pure metal which is the same regardless of the alloying element, provided that the second element is added in solution in sufficient concentration (Smallman, 1955). The temperature of deformation seems to affect texture changes in about the same way as alloying additions (Hu and Goodman, 1963).

The type and degree of texture can be determined by means of pole-figure constructions. The data for these constructions are obtained by x-ray scans of the material at several specimen-to-beam orientations.

Since cross slip is a common factor to both the stacking fault energy and texture in a metal, it would be expected that a change of stacking fault energy by alloying would be indicated by the change in rolling texture observed. This suggestion has been made by Dillamore, Smallman, and Roberts (1964).

II THEORETICAL BACKGROUND

2.1 Rolling Textures in FCC Metals

When a metal is deformed by rolling, the grains tend to rotate such that the resolved shear stress acting on them is reduced. This causes a majority of grains to approach the same orientation. The material then possesses a preferred orientation, or, a crystallographic texture. A texture is usually detectable in a metal after about 20 or 30% deformation but contains some texture due to casting and processing even before deformation. It is usually necessary to deform to amounts greater than 90% in order to study conveniently the deformation texture since below this approximate reduction some of the previous texture is still present. The texture may be described quantitatively by use of pole figures. These figures, which are stereographic projections of the poles, or normals, of the crystallographic planes, represent the orientation distribution of crystallographic planes in the grains of the metal. By analyzing the character and details of the pole figure, it is possible to describe the degree and type of texture that is present.

A pinhole x-ray photograph is an x-ray diffraction pattern of a polycrystalline specimen obtained with a Laue

camera using monochromatic radiation. When such a pattern is obtained, the Debye, or diffraction, rings which appear are the result of an aggregation of spots formed by diffraction of certain crystallographic planes. Each spot corresponds to a grain which has its planes so oriented to satisfy the given Bragg condition. In a metal whose grains are oriented randomly, the population of spots around the circumference of a Debye ring is equally distributed. When the metal contains a texture, the Debye rings are of non-uniform intensity or even discontinuous around the circumference. The low intensity or missing arcs are due to few or no grains being oriented at those positions for Bragg reflection. The degree and type of texture may be determined by this method if pinhole photographs are taken at several angles between the incident beam and the specimen.

A diffractometer counter tube measures the intensity of the diffracted x-rays from a portion of the Debye ring. In order to use this instrument for determination of preferred orientation of a rolled sheet specimen, the specimen must be rotated perpendicular to its rolling face (beta angle) so that the entire Debye ring (or arcs in the case of a textured specimen) passes through the counter window. In addition to this rotation, it is necessary to rotate the specimen about its rolling axis (alpha angle). At zero degrees alpha the plane of the specimen bisects the incident and transmitted diffracted x-ray beam.

Rotation of beta through 360 degrees at this alpha angle yields the texture distribution at the periphery of the pole figure. Rotation of alpha by, for example, 5 degrees and re-rotation of beta then yields the texture distribution at 5 degrees in from the periphery of the pole figure. By obtaining x-ray scans such as these for the alpha range from zero to 90° , the orientation distribution of crystallographic planes for the entire specimen can be found. The diffractometer goniometer is set at a constant Bragg angle, usually the angle to diffract $\{111\}$ planes in FCC metals. Stereographic analysis can then be applied to obtain the crystallographic plane most predominant at the surface of the metal and its direction which coincides to the rolling direction. This plane and direction are usually reported as $\{hkl\} \langle uvw \rangle$.

Since it has been well established that slip occurs on close-packed planes, as the $\{111\}$ in FCC metals, it should be possible to predict the type of texture that will occur. However, this has proved to be difficult because of the interaction of slip systems and the impedance to slip at grain boundaries and at dislocation entanglements.

An attempt to predict the rolling texture of FCC structures by Boas and Schmid (1931) assumed operation of three slip systems and derived stable end positions. They correctly predicted a $\{110\} \langle 112 \rangle$ for both tension and compression textures for alloys but did not explain how the

crystals which were not initially in the end positions could reach these positions. Taylor (1938) used a mathematically rigorous analysis which predicted the simultaneous operation of three to five slip systems. However, besides the limitation of his assumption of homogeneous deformation, the computations for a metal are very difficult. Pickus and Mathewson (1939) assumed unequal participation of the three most favorable glide systems. The most favorable systems were defined as those in which the product of the resolved shear stress and the cosine of the angle between the glide direction and the direction in which free flow may occur are the highest.

The above three theories all depend on the resolved shear stress on the most favorable system to become greater than the critical value until the resolved shear stress on less favorable systems becomes high enough for slip to occur.

Boas and Hargreaves (1948) suggested that multiple slip systems are required to operate only in the immediate vicinity of the grain boundary, while in the body of the grains slip occurs only on one or two planes. On this basis, they concluded that the deformation of the individual grains in a polycrystal could be considered as being closely similar to the deformation of single crystals. Since this theory simplified the analysis greatly while still predicting the textures correctly, it was perhaps a major contribution to the theory of rolling textures.

Two major difficulties still remained however. These were (a) the resolved shear stress on the primary, or most favorable slip system, still had to exceed the critical value before the resolved shear stress on a less favorable system became high enough for slip to occur and (b) the different type of texture observed in pure FCC metals could not be explained by any of the theories proposed at that time.

The first successful attempt to explain the former difficulty was made by Calnan and Clews (1950) who introduced an "effective stress axis" which was removed from the true stress axis by constraints imposed by surrounding grains. Since the effective stress axis did not coincide with the true axis, the resolved shear stress on the most favorable system would now be lower and thereby obviate the necessity of exceeding the critical value.

One of the most recent and better analyses of rolling textures is that of Dillamore and Roberts (1964). These investigators were able to overcome both of the above mentioned difficulties by assuming two stress axes, tensile and compressive, which act parallel and perpendicular to the rolling direction, respectively. By using the systems of maximum resolved shear stress for a biaxial stress system defined by the limitation that the tensile axis must be perpendicular to the compression axis, prediction of a $\{110\}$ $\langle 112 \rangle$ texture for primary slip and a series of

other textures including a $\{112\}$ $\langle 111 \rangle$ for cross slip was made. This analysis was experimentally confirmed by the observed textures and by the appearance of cross slip only in very dilute alloys and pure metals.

The qualitative evidence of correlation of texture and cross slip was certainly significant since another tool for investigating the plastic properties of metals was made available.

The $\{110\}$ $\langle 112 \rangle$ texture being a FCC alloy type is generally referred to as the "brass type" while the $\{112\}$ $\langle 111 \rangle$ texture being one of the textures reported for pure FCC metals is generally referred to as the "copper type".

The pole figures obtained by the diffractometer method can be described quantitatively, as well as qualitatively. Quantitative analyses of pole figures is possible since the intensities of the x-ray peaks can be compared with the intensity obtained from a sample of randomly oriented grains. By using values of intensities obtained from textured samples, which are multiples of the random sample, it is possible to obtain values of intensity which are reproducible.

However in order to obtain quantitative parameters from the pole figures, for the purpose of reporting data such as percent transition from one texture to another, or for reporting the amounts of textures which are present in

a metal, it is necessary to use some relationship of the intensities within the pole figure.

Smallman (1955) employed a convenient method of stating the transition of one texture to another. Using a $\{111\}$ pole figure for FCC metals, the ratio of intensities

$$\frac{I_0}{I_0 \pm I(25 \text{ or } 30^\circ)}$$

was reported as percentage transition. I_0 is the intensity at $\alpha = 0^\circ$ and $I(25 \text{ or } 30^\circ)$ is the intensity at $\alpha = 25 \text{ or } 30^\circ$. Liu and Richman (1960) and Hu and Goodman (1963) used a method essentially the same as Smallman's except that the ratio was taken of the peak height at the transverse direction to the peak height at about 20 degrees from the rolling direction (on the periphery of the $\{111\}$ pole figure).

A more quantitative treatment is offered by Bragg and Packer (1964) in which the entire pole figure is considered through calculation of pole densities. The texture is then represented by Gaussian or superposition of Gaussian orientation distributions.

Dillamore, Smallman, and Roberts (1964) find that the ratio of peak height measurement at the periphery used by Liu and Richman (1960) is a more sensitive intensity ratio than that used by Smallman (1955). The intensity peaks at about 20 degrees to the rolling direction remain

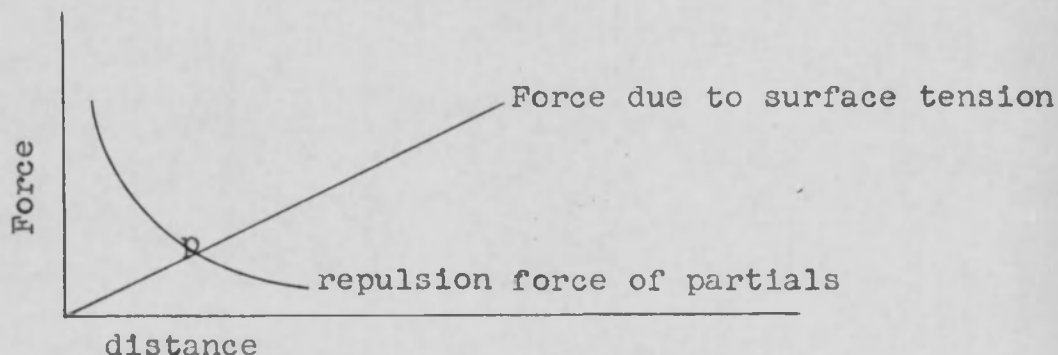
essentially stationary while the intensity peaks at the transverse direction move toward the center as the texture changes from the $\{110\}$ $\langle 112 \rangle$ (brass type) to the $\{531\}$ $\langle 112 \rangle$ (copper type).

By using the intensity ratio at the periphery, Merlini and Beck (1955) determined the copper-to-brass texture transition and found that the main components of the rolling texture gradually shift over a wide composition range from pure copper to 70-30 brass. Hu and Goodman (1963) have shown that the rolling texture of copper gradually changes from the copper-type texture to the brass-type texture as the temperature of deformation decreases. A remarkable resemblance was found in the rolling textures of copper deformed at -80, -140, and -196° C to the room temperature rolling textures of brasses containing 3, 6, and 10% zinc, respectively, as reported by Merlini and Beck (1955). Smallman (1955) investigated the texture dependence of a brass containing 5% zinc at different temperatures. At 200° C, the texture is the pure metal type, at room temperature a 40% transition to the brass type occurs, while rolling at liquid air temperature produces almost a 100% transition to the brass type.

2.2 Stacking Faults

Stacking faults in metals, as the name implies, are faults in stacking of atom layers. These faults cause a

region of higher energy compared to the usual lattice stacking and are formed when dissociation of dislocations occur. The dissociation of dislocations occurs because the energy of the dislocation is lowered by the dissociation process. When the dislocation becomes dissociated, or extended, it is split into two other dislocations called partials which are of lower energy and repel each other. The mutual repulsion of the partials creates an area in which the stacking normal to the plane of the partials has been altered from the usual FCC structure to a HCP structure. The distance between the partials is a measure of the stacking fault energy. The equilibrium distance between partials is a result of two opposing forces: (a) the tendency of the metal to be FCC rather than HCP, or the surface tension of the fault, and (b) the repulsive force caused by interaction of the stress fields of the partials which tends to separate the partials and thereby decrease the energy of the stress fields.

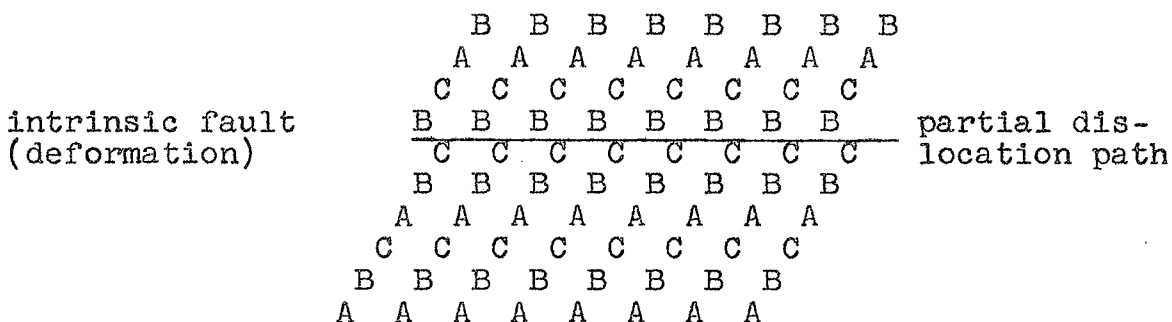
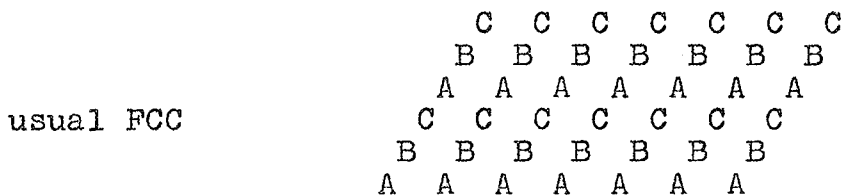


Sketch 1. Surface tension and partial dislocation repulsion vs. distance of separation of partials.

The distance at point p is the equilibrium distance between partials. For a metal of high stacking fault energy, the slope of the surface tension is steeper and therefore the stacking fault energy is higher. The lower the stacking fault energy, the greater the separation between the partials and the wider the stacking fault.

The types of stacking faults which can occur in FCC structures are due to ordering, quenching, climb by diffusion, and plastic deformation. Only the intrinsic fault caused by plastic deformation and the twin fault caused by diffusion are pertinent to this discussion. They will be described here in more detail.

The stacking sequence perpendicular to the plane of the fault can be compared schematically with the usual FCC stacking as follows:



twin fault

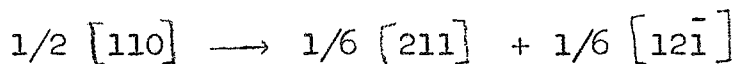
```

A  A  A  A  A  A  A  A
B  B  B  B  B  B  B  B
  C  C  C  C  C  C  C  C
    A  A  A  A  A  A  A  A
      B  B  B  B  B  B  B  B
        C) C) C) C) C) C) C) C)
          B  B  B  B  B  B  B  B
            A  A  A  A  A  A  A  A
              C  C  C  C  C  C  C  C
                B  B  B  B  B  B  B  B
                  A  A  A  A  A  A  A  A

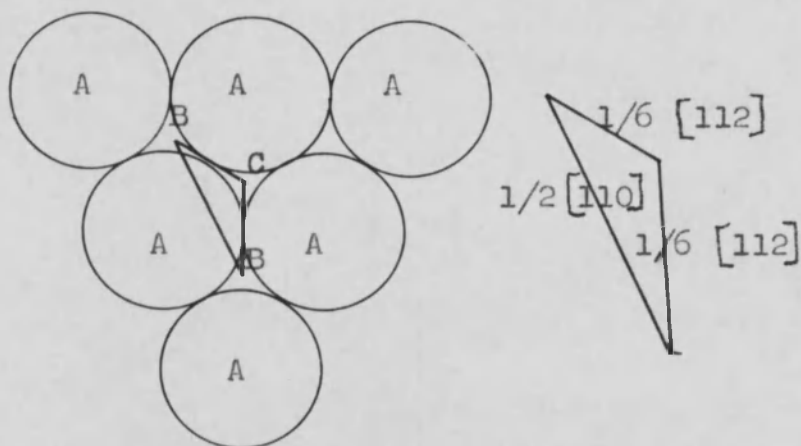
```

In the deformation fault, the A layer above the dislocation path has been changed to a B layer by the movement of atoms along a $\langle 112 \rangle$ direction so that the stacking has been changed from ABCABC..... to ABCABCBCAB..... The twin fault is thought to form during crystal growth or recrystallization.

A dislocation which lies on the slip plane may split up into two partial dislocations due to the energetically favorable reaction



where the terms in the equation indicate the magnitude and direction of the Burger's vector. The total dislocation is said to have become extended. The relation of these vectors on the close packed plane is shown below:



Sketch 2. Burger's vector relations on $\{111\}$ plane FCC Crystal.

A marble model of splitting of the dislocation is shown in Fig. 1 (a) and the resulting fault viewed perpendicular to the close packed plane is shown in Fig. 1 (b) and (c).

An annealing-twin fault is thought to form during either recrystallization or during grain growth. Mathewson (1944) has proposed a theory of the generation of twins from stacking faults during recrystallization. Fullman and Fisher (1951) have indicated that twins appear at grain corners whenever the boundaries between a parent and its neighboring grains are of higher energy than those between the twin and these neighbors, the difference exceeding the energy produced by the creation of a coherent twin boundary. The coherent twin boundary is defined as the boundary at which atoms of the twinned and parent crystal match up

perfectly across the twin boundary. Boundaries at which atoms do not match up perfectly are termed non-coherent twin boundaries.

A coherent twin boundary in FCC metals has one next-nearest violation, BCB, while a deformation fault has two such violations, BCB and CBC. The deformation fault, therefore, is assumed to be made up of two twin faults and consequently the stacking fault energy should be twice the twin boundary energy (Read, 1953).

The measurement of stacking fault energy has yielded a large discrepancy in values using either theoretical calculation or experimental values.

Seeger, Berner and Wolf (1959) made measurements of the temperature and strain rate dependence of the shear stress corresponding to the transition from linear to parabolic hardening in a single crystal stress-strain curve to deduce stacking fault energies of several metals. In this treatment the onset of stage III in the single crystal stress-strain curve is related to the stacking fault energy. The results of this treatment yielded values of stacking fault energies which are very much different from previously accepted values.

An x-ray method which determines the stacking fault probability, of frequency, has been used by several investigators (Hu and Goodman, 1963; Wagner, 1957; Davies and Cahn, 1962; Warren and Warekois, 1955, for instance). In

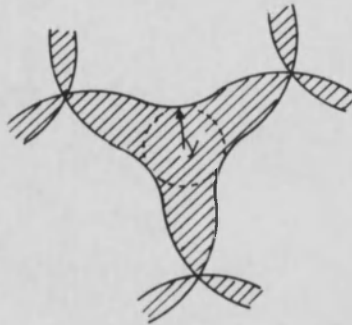
this method the peak shifts of certain planes are measured (usually the $\{111\}$ to $\{200\}$ and $\{220\}$ to $\{311\}$ planes in FCC metals). The peak shift is caused by lattice strains due to cold work and small particle sizes as well as by stacking faults. By application of Fourier analysis to the displaced and broadened peaks it is possible to determine the center of gravity and, therefore, the displacement to a fairly good accuracy. The stacking fault energy is related to the stacking fault probability as given by the relation

$$\alpha = \frac{Ga^3p}{24(2)^{1/2}E} \quad (\text{Nakajima, 1960})$$

where alpha is the stacking fault probability and G, a, p, E are the shear modulus, the lattice parameter, the dislocation density, and the stacking fault energy, respectively. In this method it is necessary to use a weighted mean of the $\{111\}$ planes responsible for reflection. This weighted mean becomes less appropriate for large stacking fault probabilities (low stacking fault energy).

The most widely accepted values of stacking fault energy are those derived from dislocation node measurements by use of the transmission technique on the electron microscope.

When three families of dislocations on the same plane intersect, a triple node configuration results:



Sketch 3. Dislocation node containing faulted area.

Each dislocation is split into two of the three possible mobile partial dislocations. On half of the nodes, the partial dislocations meet in such a way that the nodes can open up into a triangle; on the other half of the nodes, the necessary crossing over of the partials keeps the nodes closed (Friedel, 1964). The stacking fault energy is then calculated from the relation

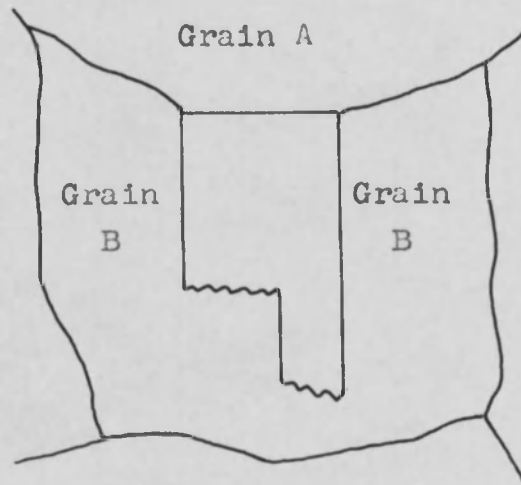
$$E = \frac{Gb^2L}{43.6\gamma}$$

where G is shear modulus
 b is Burgers vector
 L is $4.55(2+v)/(1-v)$ for edge dislocations and $5.95(2-3v)/(1-v)$ for screw dislocations
 v = Poisson's ratio
 γ is inner radius of triangles

The equation is an approximate one because the core radius of a dislocation is still uncertain and the variation of dislocation energy along the curved length is difficult to evaluate.

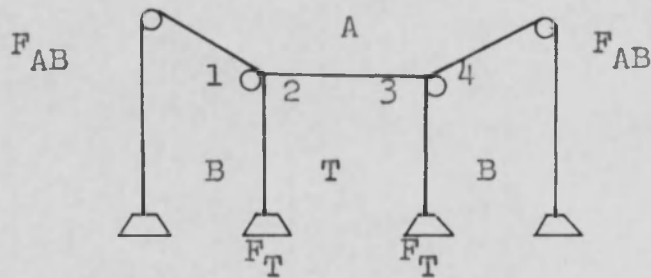
Another limitation to the dislocation node measurement is that it is only applicable to metals of low stacking fault energy. As the stacking fault energy increases, γ becomes smaller until it reaches the limit of resolution of measurement. The limit is reached at approximately 10% zinc in brass so that it is necessary to extrapolate to obtain the value for pure copper. This extrapolation assumes that the curve is continuous and follows the trend established from 70-30 brass to 90-10 brass. It would be desirable, therefore, to obtain stacking fault energies by another method in the low zinc range to determine if the extrapolation which is used is justified.

If the assumption is valid that the twin boundary energy is one-half the stacking fault energy, then the area of extrapolation could be confirmed or corrected. Only three investigators have determined twin boundary energies (Fullman, 1951; Bolling and Winegard, 1958; Inman and Kahn, 1961). Only pure metals, copper and lead, were used in these investigations, but it may be possible to extend the method to alloys. The surface tension of a twin boundary can be measured by using a mechanical analogy proposed by Fullman (1951). Consider a twin trace on a FCC crystal whose surface coincides with the $\{110\}$ plane. Since FCC metals twin on the $\{111\}$ plane, then this twin plane will be perpendicular to the surface. The surface tension of the twin boundary tends to pull the grain boundary in such a way as to shorten the length of the twin boundary:



Sketch 4. Twinned crystal

The surface tension of the twin boundary, then, may be calculated by resolution of forces parallel to the twin boundaries:



Sketch 5. Mechanical analogy of twin surface energy.

Resolving forces in the vertical direction yields:

$$\frac{F_T}{F_{AB}} = \frac{\cos\theta_2 \cos\theta_4 - \cos\theta_1 \cos\theta_3}{\cos\theta_3 - \cos\theta_2}$$

where F_T is the twin boundary energy and F_{AB} is the grain boundary energy. Bolling and Winegard (1958) used the same analysis for one-twin boundaries and employed the relation

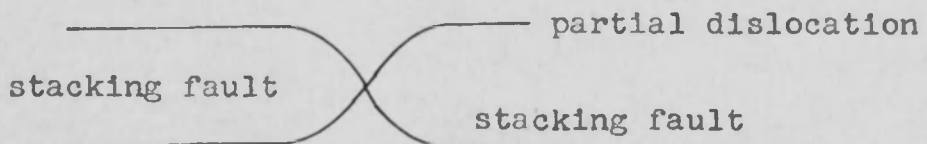
$$\frac{F_T}{F_{AB}} = -(\cos \theta_1 + \cos \theta_2).$$

It is seen from the above equation that to obtain the stacking fault energy of a material it is necessary to know the grain boundary energy. In addition the angles involved must be true dihedral angles or their orientation must be known. The grain boundary energies for the solid solution range of the Cu-Zn system have been calculated by Taylor (1958). Harker and Parker (1945) have shown that if a large number of measurements are taken, the modal value should lie within 5° of the true value. Bolling and Winegard (1958) have used this latter assumption in determining the interfacial free energy of twin boundaries in lead. Fullman (1951) used the assumption that most of the grains were oriented such that the $\{110\}$ planes were parallel to the surface.

2.3 Dependence of Texture on Stacking Fault Energy

The addition of a solute to a pure FCC metal has been found to change the texture from the copper type to the brass type (Merlini and Beck, 1955; Smallman, 1955). Prediction of the type of texture obtained has been made very satisfactorily (Dillamore and Roberts, 1964; Liu, 1964) on the basis of the cross-slip mechanism. The brass-type texture is found to predominate in alloys where cross slip is absent or where it occurs to a low extent; the copper type is predominant where cross slip occurs to a high extent.

The amount of cross slip, which changes the texture, has been attributed to the stacking fault energy of the material. The following schematic drawing illustrates why cross slip is more difficult in metals with wide stacking faults (low stacking fault energy):



Sketch 6. Stacking fault with constriction

The extended screw dislocations which are on the slip plane cannot cross slip unless they become constricted at some point. More energy is required to constrict wide faults than is required for narrow faults. Seeger (1959) assumed a model pile-up of stacking faults at Lomer-Cottrell locks. The leading dislocation becomes constricted until cross slip can occur. However, Thornton, Mitchell and Hirsch (1962) suggest that cross slip can be activated by the jogging of the glide dislocations with tangled dislocation, dipoles, and prismatic loops as well as with Lomer-Cottrell locks. Howie and Swann (1961) have indicated that the addition of zinc to copper lowers the stacking fault energy due mainly to the number of valence electrons in the alloys. Swann and Nutting (1961) have suggested that lowering the stacking fault energy by the addition of alloying elements, reduces the size of the dislocation substructure cells and thereby increases the dislocation density within the cells. The dislocation density then, will increase as cross slip decreases. The stacking fault energy, as determined by the x-ray method, is inversely proportional to the dislocation density so that the stacking fault energy should increase with the amount of cross slip. Nakajima (1960) attributes the increase of stacking fault probability with additions of solute to be due to the concentration of solute atoms around faulted layers. This was verified by small angle scattering experiments with Cu-Al alloys.

Since the texture is a function of the amount of cross slip and the amount of cross slip is a function of the stacking fault energy, then the texture should be a function of the stacking fault energy. If the stacking fault energy can be shown to follow some exponential relation with solute additions and if the same relation exists for texture versus solute additions, then the texture should vary linearly with the stacking fault energy.

Smallman and Green (1964) have shown that in Ag-Au alloys the texture changes in the same order as the stacking fault energy change. Dillamore, Smallman, and Roberts (1964) have shown that the amount of copper-type texture can be used to classify pure FCC metals in order of their stacking fault energy.

2.4 Effect of Solute Additions on Interfacial Energy

When a solute is added to a pure metal, the surface tension of a metal surface, grain boundary, or twin boundary is decreased. This decrease is due to segregation of the solute atoms to either side of the boundary because these boundaries act as a sink for the solute.

The influence of impurities, or solutes, on the interfacial energies in metals has been studied extensively from a thermodynamical approach. However, comparisons between theory and experiment have not been made to any great extent primarily because of the experimental difficulty in determining the solute concentration at the interface.

The Gibbs adsorption isotherm gives a relation between the change of surface tension of a liquid with dilute concentration of solute dy/dc , and the excess concentration of solute in the surface, Γ :

$$\Gamma = -(C/RT) (dy/dc).$$

This equation shows that, as a rule, solute elements which decrease the surface tension avoid the surface. It would be expected that this relation might be applicable to solids since solute atoms larger than the solvent atoms would replace the latter and fill up gaps at the interface while solute atoms smaller than the solvent atoms would help relieve compressive stresses (McLean, 1957).

The observed results, in metals, are that solutes lower the surface tension. Buttner, Funk, and Udin (1952) have found that the surface tension of silver decreased by a factor of approximately 3 by adsorption of oxygen. The ratio of grain boundary energy due to surface energy remained the same however. This is probably due to the grain boundary energy decreasing at the same rate as the surface tension because of pipe diffusion of the oxygen along the grain boundary.

Bragg and Nye (1947) found with the bubble model that when bubbles larger or smaller than the average size were present, a large proportion were situated at grain

boundaries. More evidence for solute segregation to grain boundaries is given by the thermal etching phenomena. This ridge-and-trough effect has been ascribed to the presence of a second element partly because it differs from the normal etching effect at a grain boundary, and also because it varies in strength with composition and heat treatment. This effect has been observed in several copper alloys (Perryman, 1953) but not in high-purity copper.

Probably the most direct evidence obtained at present for solute segregation to interfaces was obtained by use of radioactive elements introduced by Inman and Tipler (1958). This technique involves breaking of alloyed test specimens at a low temperature to obtain grain boundary fracture. Successive layers of material are then removed by etching. The etching solutions are analyzed for the radioactive element. In this way Inman and Tipler (1958) found that an addition of 0.5 w/o Pb to Cu reduced the surface energy by a factor of approximately 2. This results correlated well with the Gibbs equation.

OBJECTIVES

The objectives of this investigation were as follows:

1. To determine the twin-boundary energy of brasses in the range of 0 to 12 percent zinc.
2. To analyze the twin-boundary energy method in an attempt to determine if the stacking fault energy is twice the twin boundary energy as presently supposed.
3. To seek a quantitative correlation between stacking fault energy and rolling texture for brasses in the low zinc range.

MATERIALS AND PROCEDURE

The brasses used in this investigation were prepared from 99.999% Cu, donated by American Smelting and Refining Company, and 99.999% Zn, obtained from Consolidated Mining and Smelting Company of Canada. The chemical analysis of these materials is given in Table I.

To prepare the alloys, a master brass alloy of approximately 16.7 w/o Zn was prepared from the high-purity Cu and Zn by melting the component metals in a sealed quartz tube which was evacuated to approximately 10^{-6} mm Hg. The molten brass was mixed by shaking the tube which was immediately quenched into water. The resulting ingot, still sealed in the quartz tube, was then homogenized for one week at 816°C . From this master brass alloy, specimens of Cu-Zn alloys with zinc contents of approximately 1%, 2%, 5%, 7%, 9%, 11%, and 13% were prepared by diluting with copper and processing similarly to the master alloy.

The alloys were then chemically analyzed for Zn content by the x-ray fluorescence method using the XRD-5 GE Spectrometer. The analysis consisted of the following operations: (1) preparation of Cu and Zn liquid solutions of known concentration, (2) preparation of standard brass solutions by mixing the desired proportions of Cu and Zn solutions, (3) determination of the relation between

fluorescent intensity of Cu and Zn, (4) preparation of solutions from ingots, and (5) determination of Zn content of ingots by comparing intensities with standard curve. A detailed procedure for chemical analysis of alpha brasses in the range of 0% to 15% Zn is given in Appendix A. The alloys were analyzed for Zn content on both ends of each ingot. The analysis indicated segregation to be within an average of 0.14% of each end with a maximum of 0.37% difference occurring in one specimen. The analyses of Zn content for the alloys are shown in Table II.

For the preparation of the pole figure specimens, a sample from each ingot was rolled on a Stanat two-high cold-rolling mill with 3-inch-diameter rolls. The sheet was reversed end-to-end for each pass to minimize asymmetric pole figures. The samples were rolled to 98.3% reduction in thickness with no intermediate anneals, the sheets having a final thickness of 0.007". The grain size of the ingot before rolling was about 2 mm on the surface and cross-section. This yielded approximately 40 grains per inch in the transverse direction and 1 grain per inch in the rolling direction of the rolled sheet. Circular specimens were then punched out of the sheets, the diameter coinciding with the diameter of the x-ray specimen holder, 1-3/8". It was necessary to reduce the specimen thickness to about 0.003", giving an x-ray absorption factor of about 2, to insure adequate intensity of x-ray beam penetration through the specimens.

This was accomplished by chemical thinning in an etchant of 30% nitric acid, 20% acetic acid, and 50% water.

Pole figures were determined with a GE-XRD-5 diffractometer equipped with a Proportional-counter and an automatic pole-figure goniometer. Cu K-alpha radiation, and a Ni filter, were used in obtaining $\{111\}$ pole figures of the alloys. A detailed procedure for obtaining pole figures and the effects of the variables thereof is included as Appendix B. In this investigation no random oriented sample was used as an intensity basis since this author has found that in a sample having pronounced texture, the background intensity varies approximately linearly with random sample intensity. The iso-intensity contours are based on equal intensity increments at $\alpha = 0$ (i.e. the angle where the specimen plane bisects the angle between the incident and transmitted beam).

For the measurements of twin-boundary energy, a sample from each ingot was cross rolled on the Stanat rolling mill to induce a $\{110\}$ texture. The samples were rolled to 98% reduction in thickness with no intermediate anneals. The final thickness of the sheets was 0.009". To obtain equilibrium annealing twins, strips approximately $1/4"$ x $2-1/2"$ were cut from the cross-rolled samples, and individually sealed in a partially evacuated (50 mm Hg) $5/16"$ Vycor tubing. The specimens were then broken out of the tubing and mounted in a casting resin

(no heat or pressure applied). The ends of the specimen were bent up to provide a contact for electropolishing:



Sketch 7. Specimen mount for electropolishing

The specimens were then ground lightly on 600 grit paper and electropolished in an orthophosphoric acid solution. Etching was done with a 2 to 1 mixture of NH_4OH and H_2O_2 by swabbing.

The angles between the twin traces and the grain boundaries were measured at a large number of twin-grain boundary intersections at a magnification of 500X using a rotating mechanical stage on a Reichert metallograph. The rotary stage has a calibrated degree scale with vernier so that measurements can be made to 0.1° . The mean twin-grain boundary energy and the standard deviation were calculated for the copper and each of the brasses by the use of an IBM 7072 computer.

V RESULTS

5.1 Twin Boundary Energies

The frequency distributions of the apparent relative energies calculated from the equation $R = -(\cos\theta_1 + \cos\theta_2)$, where R is the ratio of twin boundary energy to grain boundary energy, are plotted in Fig. 2, 3, and 4. The distributions appear close to normal and are all characterized by a slight skew towards the high values of relative energy. However, for a large number of observations the mean should be normally distributed. The minimum number of observations required to obtain a mean value characteristic of the material was determined by plotting the mean and range of confidence against the number of observations as shown in Fig. 5 for a brass containing 12.88 w/o zinc. It can be seen in the figure that at approximately 100 observations, both the mean and range of confidence become essentially constant. It was assumed that this number of observations would also apply to the rest of the alloys and the pure copper. Due to time limitation and the discovery of an annealing texture effect, to be discussed, the twin boundary energies were not determined for the brasses containing 9.60 and 10.88 weight percent zinc. Values of the relative energies, along with the range of confidence are shown in

Table II. The range of confidence was determined for 90% confidence limits from the relation $u = \bar{x} \pm t_{.10} s(\bar{x})$ where \bar{x} is the mean, $t_{.10}$ is obtained from students' "t" test statistical tables for the given number of observations, and $s(\bar{x})$ is the standard error. The standard error is given by the ratio of the standard deviation to the square root of the number of observations.

By using the values of grain boundary energies calculated by Taylor (1958), the twin boundary energy was obtained for each alloy. These are plotted in Fig. 6.

5.2 Rolling Textures

Rolling textures obtained for the copper and brasses in this investigation are shown in Fig. 7 and 8 with the weight percent zinc as indicated. These pole figures are in fairly good agreement with those previously reported by Merlini and Beck (1955) shown in Fig. 9. The disagreement, due to asymmetry, with previously reported pole figures is attributed to the large grain size present in the materials used in this investigation.

The maxima shown near the center of the pole figures shown by Merlini and Beck (1955) were not plotted in Fig. 7 and 8 because these data were not used for texture determination. Since no random sample was used, the pole figure contours represent equal intensity increments determined at $\alpha = \text{zero}$.

The rolling texture of copper consists mainly of the $\{531\}$ $\langle 001 \rangle$ which is close to the previously reported texture of $\{123\}$ $\langle 412 \rangle$ by Hu and Goodman (1963). The rolling texture of the brass is $\{110\}$ $\langle 112 \rangle$ and coincides with the texture reported by Merlini and Beck (1955).

The data taken to indicate the copper-to-brass texture transition were all derived from the periphery of the pole figure where the ratio of the intensity of the maxima at the transverse direction to the intensity maxima about 20 degrees from the rolling direction was used. The maxima close to the rolling direction remain essentially constant while the maxima at the transverse direction increase in intensity with increasing zinc content. The intensity maxima located near the center in each quadrant in the pure copper correspond to some of the $\{531\}$ $\langle 001 \rangle$ poles. These maxima merge into a single maximum, by zinc additions, toward the transverse direction. The intensity at the transverse direction consequently increases. A measure of the amount of brass texture can therefore be obtained by determining the intensity ratio as described above. This method of determining texture transition is used by Dillamore, Smallman and Roberts (1964).

Intensity ratios obtained for the copper and brasses are shown in Table III. The large grain size of the samples which caused the asymmetry in the pole figures also affected the intensity ratio but the general trend is an increase

with percent zinc. This trend, shown in Fig. 10, indicates that the brass texture increases very rapidly for the first additions of zinc to copper after which the ratio of texture change is low. The rapid change in texture for low solute additions was also reported by Frois and Dimitrov (1961) who found that copper additions as low as 15×10^{-6} atomic percent in aluminum caused a change in texture.

The asymmetry of the pole figures was confirmed to be due to large grain size by comparing a pole-figure scan of copper containing small grain size to a scan of a copper specimen containing large grains. The results shown in Fig. 11 and 12 indicate that the small-grain copper has greater symmetry. The specimen containing small grain size was also of lower purity (99.99%) and indicated a lower intensity ratio.

5.3 Dependence of Texture on Stacking Fault Energy

Due to the inherent errors in the method used for determining stacking fault energy which are to be discussed and the error introduced by the large grain size in the materials used in determining texture transition, only an apparent trend in the texture dependence of stacking fault energy can be given. Since no previous quantitative correlation has been attempted for brasses, it is not possible to compare results with values from the literature.

This approximate correlation is plotted in Fig. 14 where the values of stacking fault energy used represent the best estimated values. These values are given in Table III. The value of intensity ratio for the 2.60 w/o zinc and the value of stacking fault energy for the 5.30 w/o zinc specimens were omitted from Fig. 14 because of their large deviation from the other values due to the large grain size in the former and an unknown reason in the latter.

VII DISCUSSION

6.1 Twin Boundary Energies

An annealing-twin boundary possesses an energy which is higher than the average energy of the surrounding lattice. This is confirmed by the observed tendency of the twin boundary to shorten itself by pulling at the grain boundary and also by the well-known preferential etching at these boundaries.

Values obtained for twin boundary energies of pure metals depend on several variables. These probably include (a) purity of the metal, (b) annealing atmosphere, (c) annealing temperature and time, (d) cooling rate from the annealing treatment, (e) values of grain boundary energies, (f) the angles measured at twin-grain intersections and (g) effects of annealing texture. In general, the twin boundary energy is expected to be increased by higher purity, a decrease in contaminant in heat-treating atmospheres, a lower annealing temperature or insufficient time at temperature, a slower cooling rate from the annealing treatment, and increasing deviation of the annealing texture from a $\{110\}$ type. The remaining two variables, values of grain boundary energy and measured angles, will increase or decrease the twin boundary energy depending on existing conditions.

6.1.1 Purity of Material and Annealing Atmosphere

Purity of material and annealing atmosphere affect the twin boundary energy in a similar manner to that of solute additions. Discussion of this effect is given in a later section.

6.1.2 Annealing Temperature and Time

When a thin sheet of polycrystalline metal is annealed at a high temperature for a long period of time, the grain boundaries will migrate so as to reduce their line tension (Harker and Parker, 1945). This results in having most of the grain boundaries lying perpendicular to the axis of the sheet. If equilibrium is not reached and the grain boundaries lie at some angle not perpendicular to the sheet, the apparent grain boundary energy will be lower than its equilibrium value. This would have the effect of raising the measured value of R , the ratio of twin boundary to grain boundary energy, thereby yielding a higher value of twin boundary energy.

By comparing the value of R , 0.076, for copper obtained for an annealing temperature of 715°C, in this investigation, with that obtained by Fullman (1951), 0.045, for an annealing temperature of 950°C, it appears that the annealing temperature effect is present as

discussed above. However, this assumes that all other factors are equal which is not necessarily the case.

6.1.3 Cooling Rate

If the metal is quenched from the annealing heat treatment temperature, the twin and grain boundary energies are both lowered. The energies are not necessarily lowered equally, the lowering of the grain boundary energy probably being more severe. This lowering of energy is due to impurity diffusion to the boundaries (Inman and Tipler, 1958). The general effect of this variable is to appear to increase R when the metal is quenched. Unfortunately, the cooling rate was not given by the previous investigators (Fullman, 1951; Inman and Khan, 1951) so that comparison of results on this basis is not possible. However, cooling rate might not affect R to any great extent since Flinn (1960) has reported that cooling rate varying over a wide range of temperatures does not affect the solid solution hardening.

6.1.4 Grain Boundary Energies

The experimental values reported for grain boundary energy of copper vary from 490 ergs/cm^2 (Fullman, 1951) to 640 ergs/cm^2 (Bailey and Watkins, 1950). The discrepancy of these values could possibly be due to the purity of the

copper. Bailey and Watkins (1950) used a higher purity copper, 99.998%, compared to Fullman (1951) who used OFHC copper which is of 99.98% purity.

The grain boundary energies derived by Taylor (1958) and plotted in Fig. 6, were obtained by using the value of 580 ergs/cm^2 for the grain boundary energy of copper. This has the effect of giving a lower value of twin boundary energy if it is assumed that 640 ergs/cm^2 is a preferred value.

6.1.5 Angles Measured at Twin-Grain Intersections

Although the energy of the twin boundary is higher than the surrounding lattice, its formation is a result of lowering of energy. The most accepted mechanism of twin formation is that given by Fullman and Fisher (1951) in which they propose that annealing twins form at a moving three-grain junction. As the junction moves, by the process of grain growth, the orientation across such a junction can reach the orientation required for twinning. Since the twin boundary energy is lower than the grain boundary energy, the twin formation is energetically favorable. However, this hypothesis does not explain the almost universal occurrence of twins in pairs. This twin-pair occurrence might be explained as follows:

Consider an annealing twin being formed at a three-grain junction:

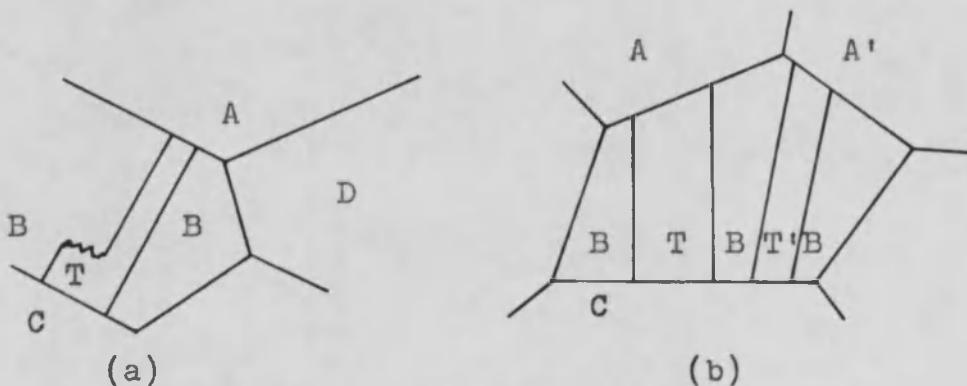


Sketch 8. Formation of annealing twin.

The energy across grain boundaries is considered to be constant except for small-angle grain boundaries where the energy is less. This has been calculated theoretically by Read and Shockley (1950) and agrees well with experimental measurements. The energy across AT, however, is not equal to the energy across AB since the boundary AT was not formed by exactly the same mechanism. According to Fullman and Fisher (1951), the energy across AT is lower than the energy across AB since observations of three-grain junctions show the angle BC is less than the 120° angle observed when the three grains are of equal energy. However, according to Smith (1950) this angle is reached when equilibrium is attained and grain growth ceases. Annealing twins would then not form from 120° grain junctions since no grain boundary movement occurs. If it is assumed that the energy across AT is actually greater than the usual grain boundary energy, then it is

possible to give a mechanism for twin-pair occurrence. The increasing energy across AT and CT, as the grain B moves toward C, would tend to inhibit the grain boundary movement as the energy along AT approaches the energy for grain boundary movement. This movement could resume if another twin boundary was formed, thereby causing the grain B to revert to its lower energy orientation. The result of this mechanism would be for twins to tend to occur in pairs which agrees with observations.

From the above discussion, the width of the twins would be a function of the orientation of T with respect to grains A and C. The energy across AT, as well as across TC, would be expected to vary depending on the twin orientation and would be lower for some orientations of T. The observed width would then be a result of an equilibrium situation, the energy due to twin width being an intermediate in energy as that across AT and across CT. Observation of twinning, in this investigation, shows at least two other cases:



Sketch 9. Some observations of twinned grains.

In the first case (a), the energy AT is greater than the energy CT. In the second case (b), the difference in width of twins is due to the difference in orientation of A and A', T and T' probably being close to the same orientation. The fact that coherent annealing-twin boundaries do not move perpendicular to the twinning plane has been shown by Fullman (1951). The non-coherent twin boundaries, however, do migrate parallel to the coherent twin boundaries (Fullman, 1951). It is possible, therefore, for the twin in case (a) to become of constant width if grain boundary movement causes the twin to extend from grain C to grain D and if the orientation of grain D is close to that of grain C.

The significance of the above discussion of occurrence of twin pairs is that a source of error in the method of computing twin boundary energies is inherent in the method used by this investigator and all previous ones (Fullman, 1951; Bolling and Winegard, 1958; Inman and Khan, 1961). In this method the force exerted on the twin boundary by the twin-to-grain boundary AT is assumed to be the usual grain boundary force while it is probably different from this value. The error is present whether it is assumed that the AT boundary is of lower energy (Fullman and Fisher, 1951) or higher energy as suggested here.

Since measurement of the energy of the AT boundary would be difficult, a better method would be to use the

relation

$$R = -(\cos\theta_1 + \cos\theta_4)$$

for determining the twin boundary energy. θ_1 and θ_4 are the angles on either side of the twin pair. This method would eliminate the use of the AT boundary energy. It would also probably eliminate the negative values of R which are common using the present method. It is inconceivable to expect that the twin boundary energy is greater than the grain boundary energy as is implied by the negative values of R. This investigator did not observe any case in which the sum of the angles on either side of the twin pair was less than 180° during a random check of about 30 twins.

6.1.6 Effects of Annealing Texture

When the angles between a twin trace and the grain boundary on both sides of the twin are measured, the measured value of R is in general higher than the true value depending on the angle of the twin surface with the perpendicular to the sheet surface. The larger the angle, the higher is the measured value of R. In the special case where the $\{110\}$ plane coincides with the specimen surface, the $\{111\}$ twin planes will lie either at 0° or 54.7° to the surface perpendicular. Four of the $\{111\}$ planes in the unit cell will lie at 0° while the other four will lie at 54.7° . Since, in compression rolling

(viz. cross rolling), the texture of the rolling sheet is predominantly of the $\{110\}$ type, Fullman (1951) assumed that by measuring only the twins with boundaries nearly perpendicular to the surface, the values of R obtained would be the true values. However, during the necessary annealing treatment after rolling, the texture is changed to a pronounced cube texture, $\{001\}$ $\langle 100 \rangle$ (Merlini and Beck, 1955, for instance). With this type of texture, all the $\{111\}$ planes in the unit cell make an angle of 35.3° with the surface perpendicular. The values obtained by Fullman, then, appear to have an inherent error due to his assumption. Although he stated that the orientation of the twinned grains was determined, the method used, that of measuring angles between slip traces, does not yield unique solutions and in fact may yield erroneous solutions (Cullity, private communication). To determine grain orientation by means of slip and twin traces, four octahedral traces are required (Takeuchi, 1959). This has proved unattainable by this investigator, on copper and brasses, regardless of the amount of deformation introduced.

The same assumption was used by Bolling and Winegard (1958) in their investigation of annealing twins in lead. Although the annealing texture of lead might yield a pronounced texture in which both the twins and grains are perpendicular to the sheet surface, the occurrence of this seems unlikely. Inman and Khan (1961) circumvent the

texture limitation by use of transmission-electron microscopy. In this method, electron-diffraction patterns of the twinned crystals are used to determine the orientation of each twinned grain in which the twin angles have been measured.

In this investigation, it was assumed that a pronounced cube texture was present in the copper and brass specimens. For the copper, this was confirmed by a pole-figure scan of a specimen that had been annealed at the same temperature and for the same time as the specimen from which the twin angles were measured. For the brasses, however, the assumption probably leads to erroneous values of R , since Merlini and Beck (1955) find that the decrease in the amount of cube texture is very great between 0 and 3% zinc, and it is also quite considerable between 3 and 6% zinc, while in a 10% zinc brass, the amount of cube texture is very low. Due to the radical change in annealing texture in these low-zinc brasses as shown by Merlini and Beck (1955), it would be difficult to make the necessary correction of R . The values plotted in Figure 6 for R and twin boundary energies are the values that were measured, without correcting for the texture effect. However, since the cube texture decreases with percent zinc, it is reasonable to assume that the angle of the $\{111\}$ twin traces with the surface perpendicular increases as the high index annealing texture components

(e.g. $\{214\}$, $\{358\}$), reported by Merlini and Beck (1955), increase. This has the effect of increasing the measured value of R . Fig. 6 should then actually show a decrease of R with percent zinc rather than the approximately constant value of R .

For the copper, the value of R could be corrected by use of the relation

$$R = R' \cos 35.3^\circ = 0.816R',$$

where R' is the measured value and 35.3° is the angle between all the $\{111\}$ twin planes and the surface perpendicular in the case of a pure cube texture. This yields a corrected value of R of 0.0618 for a twin boundary energy of 35.8 ergs/cm² as opposed to the measured R of 0.076 for a twin boundary energy of 43.5 ergs/cm², using the value of 580 ergs/cm² for the grain boundary energy as given by Taylor (1958).

6.2 Effect of Solute Addition on Twin Boundary Energy

The effect of a solute addition is to lower the twin boundary energy due to segregation of solute atoms to either side of the boundary. The largest effect occurs at the first additions up to about 1 atomic percent zinc in brass as indicated in Figure 6. In this range, R drops by a factor of about 1.8. This expected large decrease at low concentration is supported by the results of McLean,

Inman, and Tipler (1961), who reported an energy reduction at the grain boundaries of copper when 1 weight percent Pb was added.

The most obvious mechanism for causing the large decrease in surface tension is that of saturation of solutes at the interface. If an estimate of the number of solute atoms necessary to saturate each atom plane of every dislocation, grain boundary, and twin boundary is calculated, the total impurity content necessary for saturation will be rather low. For example, in a cubic centimeter block of copper having 10^8 dislocation lines per cm^2 , a grain size of 0.06 mm, and 5 twins per grain, the atomic percent of solute needed to produce a monatomic solute layer on each interfacial plane and dislocation line is

$$\frac{\text{atoms/dislocation line} + \text{atoms/grain boundary} + \text{atoms/twin boundary}}{\text{atoms/cm}^3}$$

which yields about

$$\frac{4 \times 10^{15} + 160 \times 10^{15} + 480 \times 10^{15}}{6 \times 10^{22}} = \frac{644 \times 10^{15}}{6 \times 10^{22}}$$

or approximately 1.07×10^{-4} atomic percent.

Although the curve of R vs w/o zinc shown in Figure 6 indicates a knee at 1 w/o zinc, the actual knee could be at lower values of zinc. It would seem, therefore, that the twin boundary energy decreases until solute saturation is

reached after which the energy decreases at a slower rate due to other mechanisms such as elastic interaction of solutes with the solvent lattice and electronic disturbances.

With reference to the above discussion, the relative importance of these effects may be estimated as follows:

1. Purity increases the value of R by about a factor of 2 from OFHC (99.98%) copper to 99.999% copper.

2. Annealing atmosphere decreases R as a function of the impurity concentration of the surroundings by probably only a slight amount, providing the atmosphere is relatively clean.

3. Annealing temperature and time increase R but not to any great extent for any values obtained since the temperature and time are considered adequate for formation of equilibrium twins.

4. Cooling rate from the annealing treatment decreases R to a small extent if a slow rate is used.

5. The suggested correction on the method of measuring R affects the mean value of R by an unknown amount.

6. The annealing-texture effect yields values which are too high by a factor of 0.816 when it is assumed that a $\{110\}$ texture predominates. This effect probably becomes more serious for brasses.

The purity, method of measuring R, and annealing texture are therefore considered the principal factors which contribute to variation in the values of R.

From the above discussion, it appears that the true values of twin boundary energy for copper and brasses remain to be determined. The method used by Inman and Khan (1961) is probably the best approach to this type of determination. The optimum values for R could be determined by measuring twin angles and determining the twinned grain orientation by use of transmission-electron microscopy and utilizing the suggested correction of choosing only the exterior angles of the twins.

The present value of twin boundary ratio, 0.02, for OFHC copper as determined by Inman and Khan (1961) is probably too low while the value determined by Fullman (1951) of 0.045 is probably too high. The true value probably lies within these two values. A rough estimate is 0.03 for OFHC copper. For high-purity copper, the value is about twice the value for OFHC copper.

6.3 Twin Boundary Energy vs Stacking Fault Energy

The twin boundary energy is a measure of the energy associated with the free energy of the twin fault surface. This free energy is also proportional to the radii of curvature at dislocation nodes, where it is assumed that the repulsion of the partial dislocations is equal to the free energy of the stacking fault (Friedel, 1964).

should be lower than the stacking fault energy. At present, hardly any information is available on the effects of temperature on stacking fault energy except by the texture dependence, in which a decrease in stacking fault energy with a decrease in temperature is indicated.

6.3.3 Atom-neighbors Effect

One approach to the effect of the violation of neighboring atom stacking due to faulting would be to consider the change in distance of like atoms and obtain some value akin to the configurational entropy.

In all three cases: usual stacking, twin fault stacking, and deformation fault stacking, the distance between nearest neighbors is the same. The distance between next-nearest neighbors, however, is different between the two types of faults. In the deformation fault, the B atoms are closer together than in the usual stacking by a factor of $2/3$, the A atoms are farther apart by a factor of $3/5$, and the C atoms are closer together by a factor of $2/3$. In the twin fault, the B atoms are closer together by a factor of $2/3$, the A atoms are farther apart by a factor of $3/4$ and the C atom distance remains unchanged.

Strictly on the basis of the above difference between a twin and a deformation fault, the fault energy should differ by a factor obtained from the A and C atom

separation differences. The ratio of like-atom separation factor between a stacking fault and a twin fault is then

$$\frac{\text{Stacking fault}}{\text{Twin fault}} = \frac{3/5}{3/4} \times \frac{3/2}{3/2} \times \frac{3/2}{3/3} = 1.2$$

the three factors being related to the A, B, C atom separation distance, respectively.

The products of the individual factors rather than the sum have been used here only on an intuitive basis. The entropies of a system are usually additive but these factors are intimately interrelated with each other. In addition, the factor for the B atoms remains unchanged and a summation of factors would cause an additive term of unity to be introduced.

The only other approach to this type of analysis seems to be that of using the entropy relation:

$$S = k \ln W,$$

where k is the Boltzman constant and $W = \frac{N!}{(N-n)! n!}$.

However, the variables for the factorial terms would be difficult to choose to fit this system.

6.3.4 Electronic Effect

Seeger (1957) has stated that as a result of next-nearest neighbor violations, the energy of the electron gas (Fermi energy, E_f) changes due to the change in wave

vectors near a Brillouin zone boundary. This change must be such that the introduction of a stacking fault results in an increase of energy.

For a twin fault, the difference in Fermi energy for the copper matrix and the twin boundary should be proportional to the twin boundary energy. For a deformation fault, which consists of two twin faults, the Fermi energy increase at the fault should be due to a superposition of the two twin faults as shown in Sketch 10. The Fermi energy is shown as a continuous function across the fault but having a maximum at the fault. A rapid decrease on each side of the fault is shown to indicate the tendency for the Fermi energy to be constant.

Graphical superposition of the amplitudes of E_F for the individual twins yields a factor of about 1.75 for the electronic effect. This superposition indicates that the deformation fault energy is 1.75 times greater than the twin boundary energy.

Since the conductivity is decreased by the presence of the twin boundary because of the increase in E_F , the magnitude of the change in E_F should be indicated by electrical resistivity measurements. Indications that the conductivity does in fact drop across twin boundaries have been obtained by Hancock, Keating, and Murphy (1963).

6.3.5 Summation

Neglecting the unknown temperature effect and using the suggested approximate value for OFHC copper (p. 51) the stacking fault energy as determined from twin boundary measurements is approximately

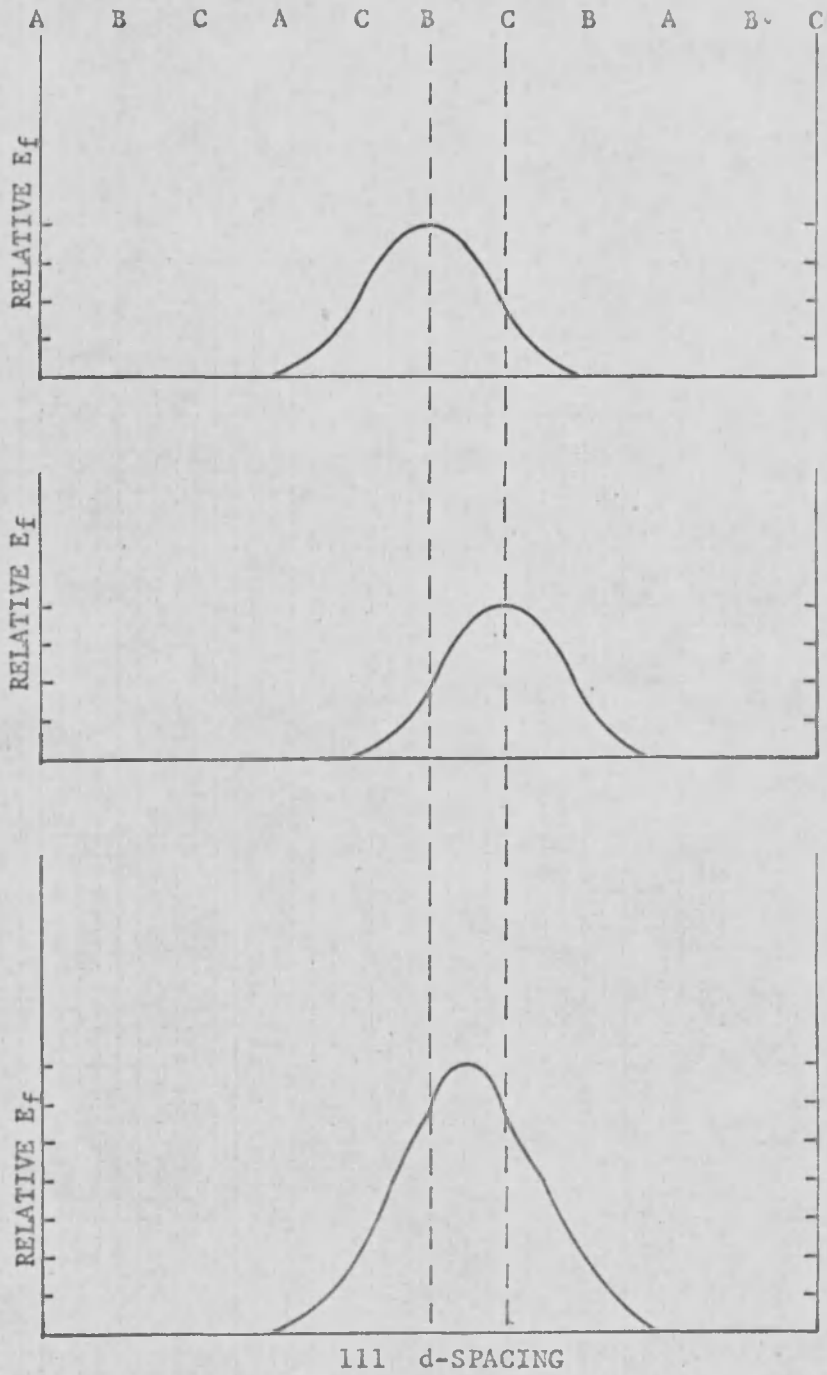
$$(0.03)(580)(1.2)(1.75) = 36.5 \text{ ergs/cm}^2.$$

For high purity copper this becomes about twice as much or about 73 ergs/cm² which agrees with the value obtained in this investigation of

$$(0.062)(580)(1.2)(1.75) = 75.6 \text{ ergs/cm}^2.$$

It is possible that the error from using the previously mentioned angles in the twinned crystal will affect this value.

The estimated values of stacking fault energy determined using all the corrections described are shown in Table III along with the values obtained by dislocation node measurements. The values by the latter method were obtained from Smallman and Green (1964) who used the Siems correction (1961) on the data obtained by Howie and Swann (1961) on 99.999% purity copper and zinc. The values obtained by the two methods are plotted in Fig. 13 where it is seen that the comparison is quite satisfactory at the overlap region of the two methods. It is believed by



Sketch 10. Schematic plot of Fermi energy vs 111 d-spacing.

this author that the values between 0 and 10 percent zinc are given more accurately by the method involving twin boundary energies.

If the factors involving the accuracy of twin boundary energies are considered for the brasses, as is possible by use of the electron-transmission-microscopy technique of determining the orientation of the twinned grains, it should be possible to obtain accurate and reliable data for stacking fault energies.

6.4 Texture Intensity Ratios

The intensity ratio used in determining texture transition is independent of the experimental conditions such as beam slits or tube power, and absorption factor. It is dependent on the (a) percent reduction, (b) grain size, and (c) purity of the specimen.

Braybrook and Calnan (1957) have shown that at high reductions, about 97 to 99%, the amount of texture increases very rapidly with increasing reduction. Consequently, a very small difference in percent reduction would affect the intensity ratio. In this investigation, the ingots were in the form of cylinders before the rolling operation so that some error in the percent reduction could have been introduced. The brass specimen containing 2.60 w/o zinc deviated by a large amount from the other values of intensity ratio due to this reason or due to its large grain size.

Grain size has been reported to have little or no effect on the intensity ratio by Dillamore, Smallman, and Roberts (1964), for the range of grain size from 10 μm^2 to 1500 μm^2 . The grain size for the materials used in this investigation was approximately 2 μm^2 . Unless the grain size causes very much asymmetry the intensity ratio should not be significantly changed. The 2.60 percent zinc specimen, however, had a very large grain size, approximately 2 cm^2 . This large grain size is probably the principal factor which caused such a large deviation of the intensity ratio in that specimen. The values for the other specimens were probably also affected by the grain size although to a lesser extent.

The effect of purity on intensity ratio can be seen in Fig. 11 and 12. The 99.99% copper yielded an intensity ratio which is greater than the 99.999% copper by a factor of approximately 2.

6.5 Effects of Stacking Fault Energy on Rolling Textures

The analysis of Dillamore and Roberts (1964) has shown that the brass-type texture is due to primary and conjugate slip while cross slip produces a copper type texture. Seeger (1957) has attributed the ease with which cross slip can occur, at a given temperature, to the width of separation of partial dislocations and hence to the stacking fault energy. The fundamental factor governing

the change in rolling texture from the copper to the brass type would then be expected to be the decrease in stacking fault energy.

6.5.1 Rolling Texture vs Cross Slip Mechanism

In analyzing the texture development, the assumption of Boas and Hargreaves (1948) that deformation mechanisms of individual grains can be considered to be closely related to those operating in a single crystal, has simplified the prediction of textures. Using this assumption, Dillamore and Roberts (1964) have shown that the absence of cross slip results in a pure brass texture. Employing the method of brass texture component in a brass specimen by using the intensity ratio described earlier, an indication of the amount of cross slip occurring can be obtained. As the intensity ratio decreases, the amount of cross slip increases.

To cause cross slip to occur in alpha brass of high zinc content, it would be necessary to apply a very high stress because of the high stability of the brass texture. This high stability has been shown by Dillamore and Roberts (1964) to be due to the fact that a large rotation of the stress axes would have to occur.

The results shown in Fig. 10 indicate a small amount of cross slip for the brass containing 12.88 w/o zinc having an intensity ratio of 1.2 and a large amount

of cross slip for the pure copper with an intensity ratio of 0.2. Furthermore, the figures indicate that the difference in amount of cross slip occurring is greater between 0 and 1 w/o zinc than it is between 1 w/o and 12 w/o zinc. This would seem to indicate that the impurity content in pure metals is a major factor in affecting cross slip.

6.5.2 Cross Slip Mechanism vs Stacking Fault Energy

When a screw dislocation moves across the slip plane it may encounter an obstacle such as an inclusion, dipoles, prismatic loops, or dislocation entanglements. These have the effect of impeding slip thereby resulting in dislocation pile ups. If the piled up dislocations are not extended it is possible for them to loop around the obstacle and resume their movement by leaving a looped portion around the obstacle. If the dislocation can move to another slip plane, or cross slip, then this will occur since this produces a path of lower resistance. On the other hand, if the dislocations are extended, cross slip becomes more difficult because the partial dislocations must form a constriction before cross slip can occur. The wider the separation between partials, the greater will be the stress required to constrict the fault. This indicates that a metal with wide faults, or low stacking fault energy, will not cross slip as readily as a metal with narrow faults, or high stacking fault energy.

The results shown in Fig. 13 suggest that adding zinc to copper lowers the stacking fault energy indicating a decrease in amount of cross slip with zinc content. The character of decrease as shown by this investigation emphasizes that the amount of cross slip which occurs is very sensitive to the initial solute additions.

6.5.3 Rolling Texture vs Stacking Fault Energy

Since both the stacking fault energy and the amount of copper texture decrease in a similar manner with zinc additions to copper it may be postulated that the change in rolling texture is due to a change in stacking fault energy.

Fig. 14 shows that the decrease of intensity ratio with stacking fault energy is not linear in the range of brasses from 0 to 12.88 w/o zinc. However, the discrepancies in both the values of intensity ratios and stacking fault energies could affect this correlation. A linear correlation would not necessarily be expected, even if the amount of cross slip were a linear function of stacking fault energy, because the intensity ratio could be an exponential function of the amount of cross slip. The lack of linearity in the logarithmic plot shown in Fig. 14 could be related to the discrepancies in the experimental values.

It would be naive to attempt a mathematical correlation using the experimental values obtained in this investigation but it is indicated that the rolling texture is definitely a function of stacking fault energy.

VII SUMMARY

Twin boundary energies were determined for high-purity copper and high purity brasses in the range of 1 weight percent to 12.88 weight percent zinc. The factors involved in the accuracy of the values obtained in this and previous investigations were considered. These factors are (a) purity of material, (b) annealing atmosphere, temperature, and time, (c) cooling rate from annealing treatment, (d) values of grain boundary energies, (e) angles selected for measuring, and (f) effects of annealing texture. Of these, (a), (d), and (e) are considered the most important.

The effect of zinc additions to copper was found to lower the twin boundary energy at a rapid rate for the initial zinc additions. After approximately 1 w/o zinc addition, the twin boundary energy remains essentially constant or decreases at a slow rate.

Analysis showed that the stacking fault energy is related to the twin boundary energy by a factor of about 2.1 which agrees closely with the present assumption, in the literature, that the stacking fault energy is twice the twin boundary energy. The stacking fault energies found in this investigation agree with values determined

by the method of measuring radius of curvature of dislocation nodes. The values disagree, however, with those in the extrapolated region of the latter method.

Rolling textures for copper and brasses were determined by pole figure analysis and were found to agree generally with previously reported ones. However, an asymmetry in the pole figures was present in the results of this investigation. This asymmetry was attributed to the large grain size present in the rolled condition.

A quantitative parameter was obtained from the pole figures by using the ratio of intensity at the transverse direction to the intensity approximately 20° to the rolling direction. This parameter was plotted against values obtained for stacking fault energies and a trend was obtained which indicated that the rolling texture is a function of stacking fault energy.

The values of stacking fault energy determined in this investigation could be ameliorated by eliminating the measurement of interior angles in twins through the use of the electron transmission microscope technique to measure the angles and determine orientations of the twinned grains. In addition if the grain boundary energies for the brasses could be experimentally determined, the accuracy of values for stacking fault energy would be further improved.

VIII CONCLUSIONS

From the results obtained in this investigation, the following conclusions have been drawn:

8.1 Twin Boundary Energies

It is possible to determine twin boundary energies for copper and alpha brasses using the method involving measurement of twin boundary dihedral angles.

This method, as used in this investigation, as well as by Inman and Khan (1961), Fullman (1951), and Bolling and Winegard (1958) contains an error in assuming that the grain boundary energy is equal to the twin-to-grain boundary energy. The latter authors -- Fullman, Bolling and Winegard -- are believed to have an additional error in their data. The former assumed a $\{110\}$ texture was present while it is fairly well known that the copper annealing texture is of the $\{001\}$ type. The latter assumed that the dihedral angles measured were true angles.

8.2 Stacking Fault Energies

The twin boundary energies determined by the above method can be used to obtain the stacking fault energy contrary to the conclusion of Thornton, Mitchell, and

Hirsch (1962). The twin boundary energy was found to be related to the stacking fault energy by a factor which is approximately 2.1.

The purity of the copper affects the stacking fault energy significantly. This may account for some of the variations in this value among several authors.

Experimental values of stacking fault energies obtained in this investigation agree well with corresponding values obtained from corrected dislocation-node measurements by Howie and Swann (1961). They disagree with those in the extrapolated region of the latter method. The values obtained in this investigation for this region are believed to be more reliable than those obtained by extrapolation.

8.3 Effect of Stacking Fault Energy on Rolling Texture

The rolling texture has been found to be dependent on the stacking fault energy for the range of brasses between 0 and 12.88 w/o zinc. Discrepancies present in both experimentally determined parameters preclude a mathematical correlation.

IX REFERENCES

- Bailey, G. L. J., Watkins, H. C., Proc. Phys. Soc. B, v. 63, p. 350, 1950
- Boas, W., Schmid, E., Z. Tech. Physik, v. 12, p. 71, 1931
- Boas, W., Hargreaves, M. E., Proc. Roy. Soc., V. 193, p. 96, 1948
- Bolling, G. F., Winegard, W. C., Jour. Inst. Metals, v. 86, p. 492, 1958
- Bragg, R. H., Packer, C. M., Jour. Appl. Phys., v. 35, p. 1322, 1964
- Bragg, W. L., Nye, J. F., Proc. Roy. Soc., v. 190, p. 477, 1947
- Braybrook, R. F., Calnan, E. A., Jour. Inst. Metals, v. 85, p. 11, 1956
- Brick, R. M., Cold Working of Metals, ASM, Cleveland, Ohio, p. 99, 1949
- Buttner, F. H., Funk, E. R., Udin, H., Jour. Phy. Chem., v. 56, p. 657, 1952
- Calnan, E. A., Clews, C. J. B., Phil. Mag., v. 41, p. 1085, 1950
- Dillamore, I. L., Roberts, W. T., Acta Met., v. 12, p. 281, 1964
- Dillamore, I. L., Smallman, R. E., Roberts, W. T., Phil. Mag., v. 9, p. 517, 1964
- Davies, R. G., Cahn, R. W., Acta Met., v. 10, p. 621, 1962
- Flinn, P. A., Strengthening Mechanisms in Solids, ASM, Cleveland, Ohio, 1960

- Friedel, J., Dislocations, Addison-Wesley Publishing Co., Reading, Massachusetts, 1964
- Frois, C., Dimitrov, O., Comptes Rendes, T 252, No. 10, p. 1465, 1961
- Fullman, R. L., Jour. Appl. Phy., v. 22, p. 448, 1951
- Fullman, R. L., Fisher, J. C., Jour. Appl. Phy., v. 22, p. 1350, 1951
- Hancock, J. R., Keating, K. L., Murphy, D. J., AEC Report, Dept. Met. Engr., Univ. Ariz., 1963
- Harker, D., Parker, E., Trans. ASM, v. 34, p. 156, 1945
- Howie, A., Swann, P. R., Phil. Mag., v. 6, p. 1215, 1961
- Hu, H., Goodman, S. R., AIME Trans., v. 227, p. 627, 1963
- Hu, H., Sperry, P. R., Beck, P. A., Jour. of Metals, AIME Trans., v. 194, p. 76, 1964
- Inman, M. C., Khan, A. R., Phil. Mag., v. 6, 1961
- Inman, M. C., Tipler, H. R., Acta Met., v. 6, p. 73, 1958
- Kittel, C., Introduction to Solid State Physics, John Wiley and Sons, New York, 1956
- Liu, Y. C., Richman, R. H., AIME Trans., v. 218, p. 689, 1960
- Mathewson, C. H., Trans. ASM, v. 32, p. 38, 1944
- McLean, D., Grain Boundaries in Metals, Oxford, 1957
- Merlini, A., Beck, P. A., AIME Trans., v. 203, p. 385, 1955
- Nakajima, K., The Research Inst. for Iron, Steel, and Other Metals, Tohoku University, 1960
- Perryman, E. C. W., J. Metals, v. 5, p. 906, 1953
- Pickus, M. R., Mathewson, C. H., Jour. Inst. Metals, v. 64, p. 237, 1939

- Read, W. T., Jr., Dislocations in Crystals, McGraw-Hill Book Co., New York, 1953
- Read, W. T., Shockley, W., Phys. Rev., v. 78, p. 275, 1950
- Seeger, A., Dislocations and Mechanical Properties of Crystals, John Wiley, New York, 1957
- Seeger, A., Berner, R., Wolf, H., Z. Physik, v. 155, p. 247, 1959
- Siems, R., Delavignette, P., Amelinckx, S., Z. Phys., v. 165, p. 502, 1961
- Smallman, R. E., Jour. Inst. Metals, v. 84, p. 10, 1955
- Smallman, R. E., Green, D., Acta Met., v. 12, p. 145, 1964
- Takeuchi, S., Honma, T., Ideka, S., Tohoko University Research Inst., Ser. A, v. 11, p. 81, 1959
- Taylor, G. I., Jour. Inst. Metals, v. 62, p. 307, 1938
- Taylor, J. W., Jour. Inst. Metals, v. 86, p. 456, 1958
- Thomas, G., Jour. of the Australian Institute of Metals, v. 8, p. 80, 1963
- Thornton, P. R., Mitchell, T. E., Hirsch, P. B., Phil. Mag., v. 7, p. 1349, 1962
- Wagner, C. N. J., Acta Meta, v. 5, p. 477, 1957
- Warren, B. E., Warekois, E. P., Acta Met., v. 3, 1955

TABLE I
 DETAILED CHEMICAL ANALYSIS OF HIGH PURITY COPPER AND ZINC
Major Impurities a/o*

Material	<u>Sb</u>	<u>Pb</u>	<u>Sn</u>	<u>Ni</u>	<u>As</u>	<u>Te</u>	<u>Se</u>	<u>S</u>	<u>Others</u>
99.999 + Cu	.0001	.0001	.0001	.0001	.0002	.0002	.0001	.0001	.00017

Parts per Million

	<u>Al</u>	<u>Cd</u>	<u>Ca</u>	<u>Cu</u>	<u>Pb</u>	<u>Mg</u>	<u>Mn</u>	<u>Si</u>	<u>Fe</u>
99.999 + Zn	.1	1.	.3	.1	1.	.1	.1	.3	.8

*Reported by suppliers

TABLE II

DATA ON TWIN BOUNDARY ENERGY

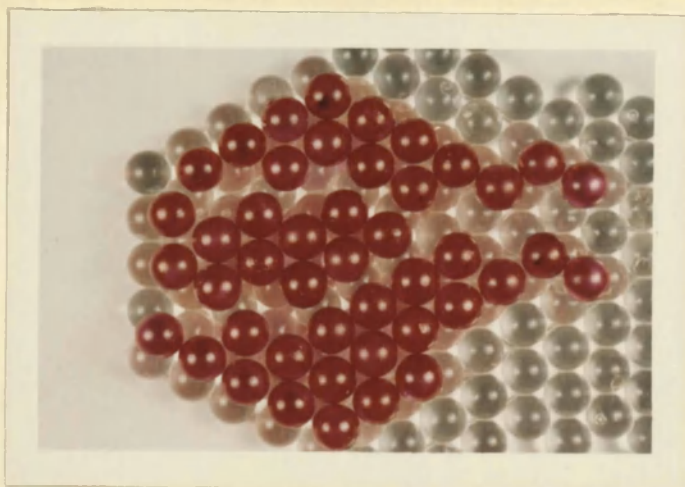
Chemical Analysis, w/o Zn	Twin/Grain Energy $\pm t_{.10} s(\bar{x})$	Grain Boundary Energy ergs/cm ² (Taylor, 1958)	Twin Boundary Energy, ergs/cm ²
0	0.076 \pm .014	580	44.1
1.03	0.042 \pm .012	565	23.8
2.60	0.041 \pm .009	558	22.9
5.30	0.035 \pm .001	553	19.3
6.85	0.043 \pm .015	550	23.6
9.60	- -	549	-
10.88	- -	548	-
12.88	0.039 \pm .001	547	21.3

TABLE III

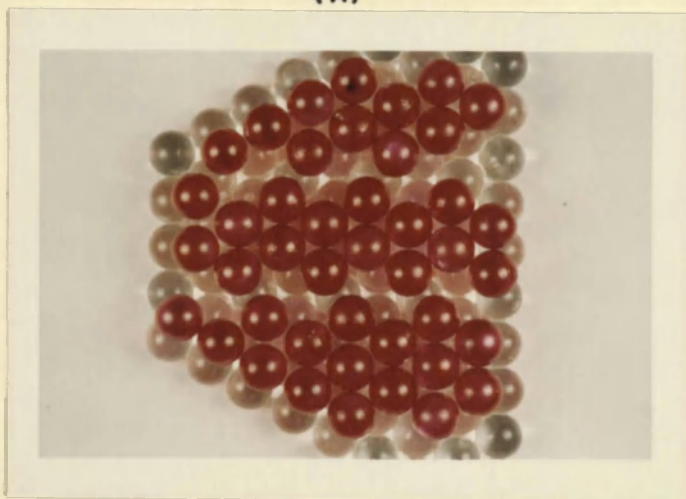
TEXTURE PARAMETERS AND STACKING FAULT ENERGIES

w/o Zn	Intensity Ratio	Ln Intensity Ratio	SFE=R(GBE)(Cos 35.3)(1.2)(1.75)	SFE (Howie & Swann, 1961)
0	0.23	-1.47	74.5	-
1.03	0.62	-0.48	40.8	-
2.60	0.17	-1.77	39.2	-
5.30	0.55	-0.60	33.1	-
6.85	0.89	-0.12	40.4	-
9.60	0.71	-0.34	-	-
10.88	0.85	-0.16	-	38
12.88	1.19	0.17	36.6	36
15.0	-	-	-	31
20.0	-	-	-	18
25.0	-	-	-	13
30.0	-	-	-	11

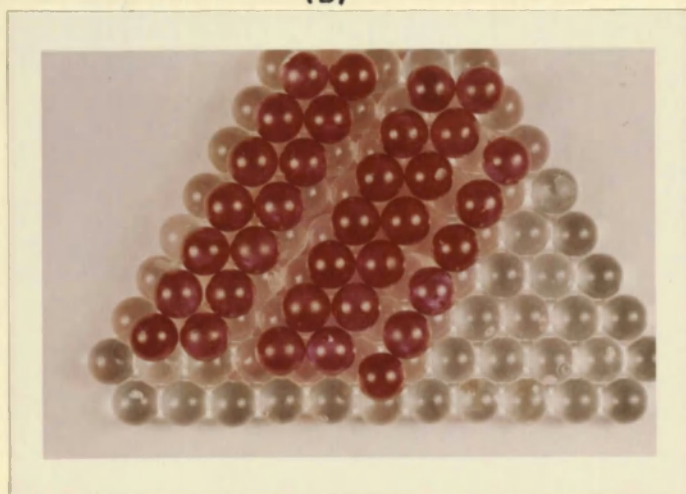
Fig. 1. Ball model of (a) splitting of total dislocation into partials; (b), (c) resulting fault.



(A)



(B)



(C)

Pages 75 through 77 do not exist.

(error made in typing page numbers).

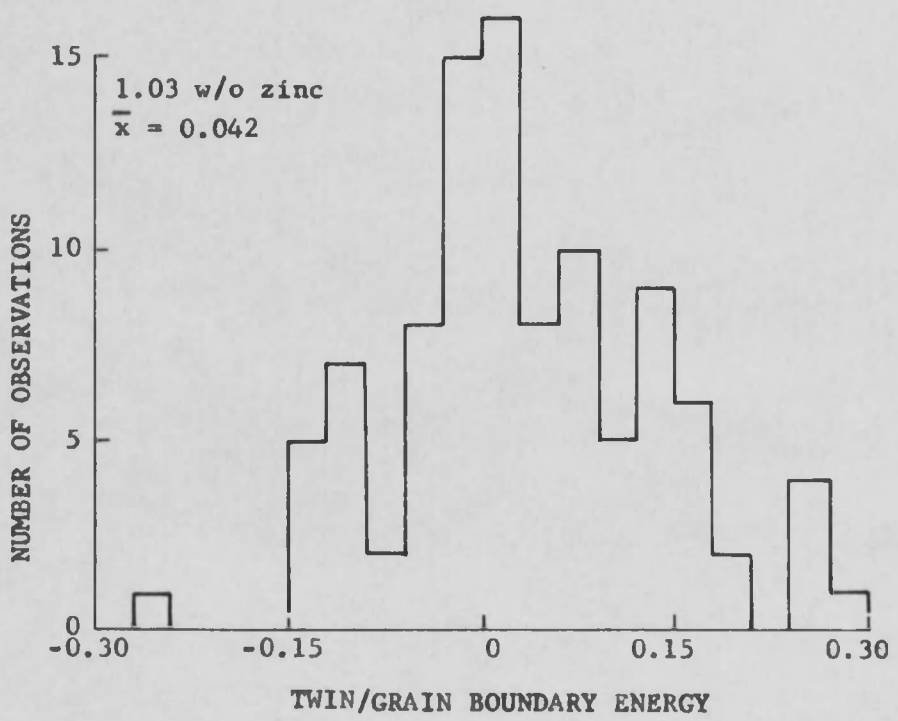
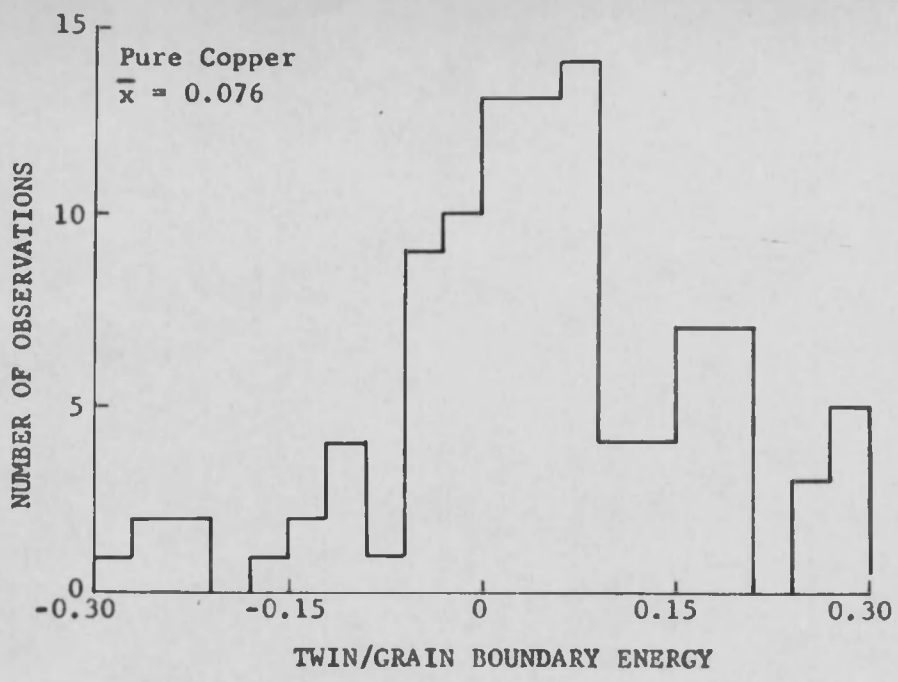


Fig. 2. Distribution of values of twin/grain boundary energy for pure copper and 1.03 w/o zinc in brass.

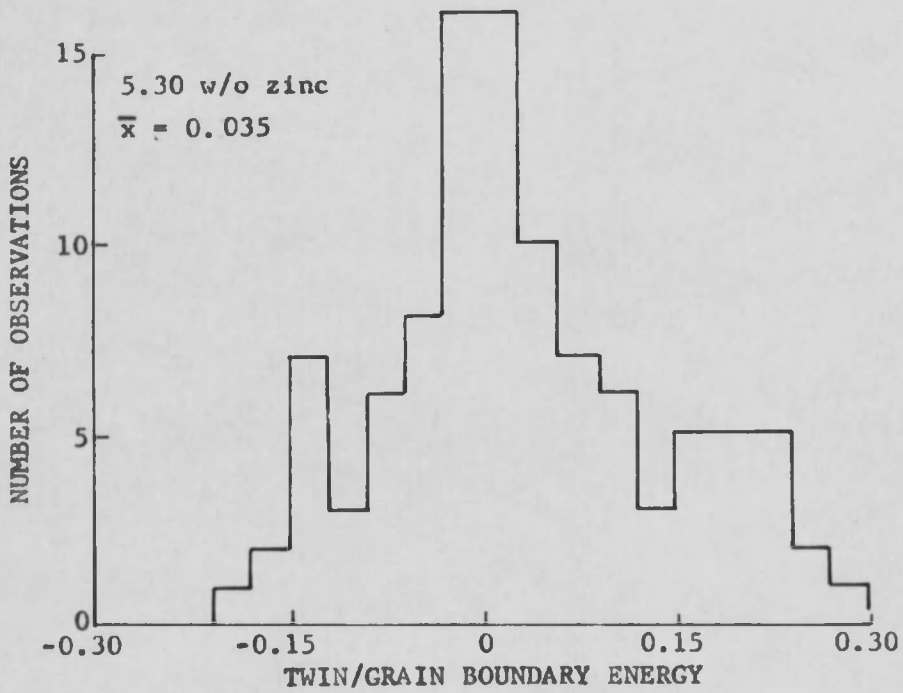
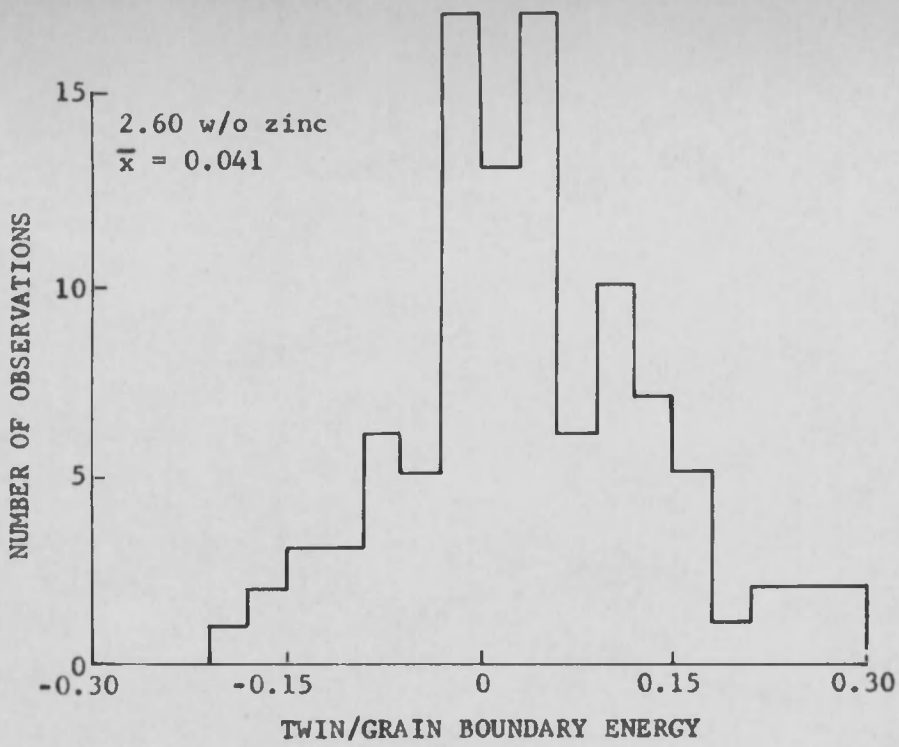


Fig. 3. Distribution of values of twin/grain boundary energy for 2.60 w/o zinc and 5.30 w/o zinc in brass.

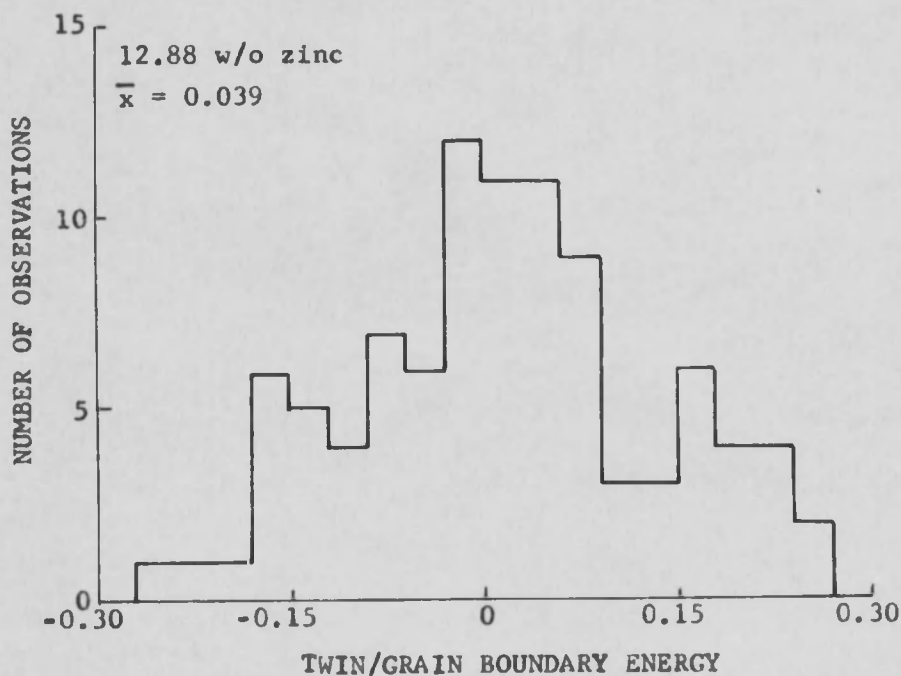
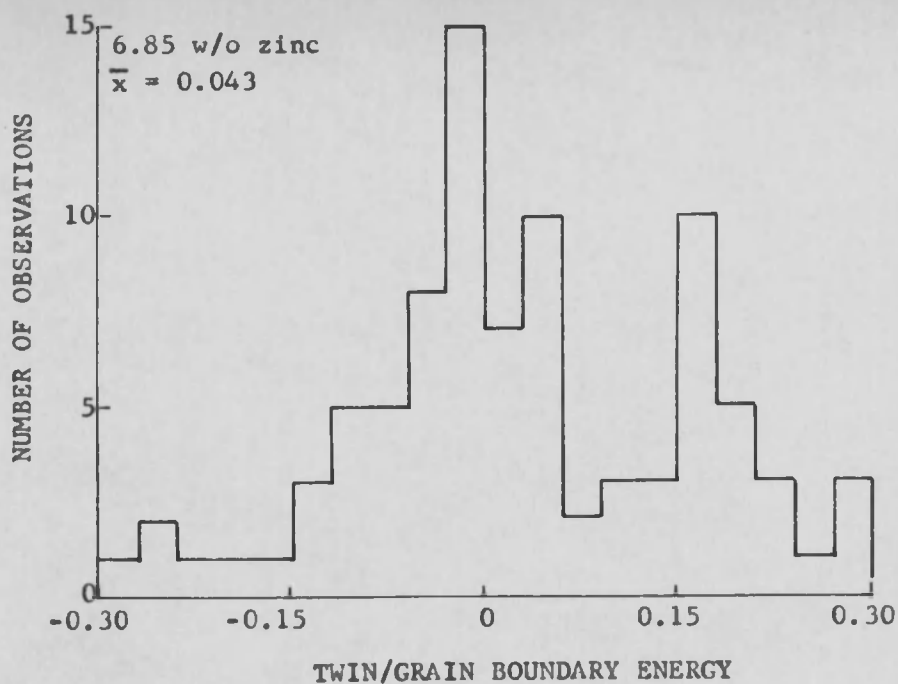


Fig. 4. Distribution of values of twin/grain boundary energy for 6.85 w/o zinc and 12.88 w/o zinc in brass.

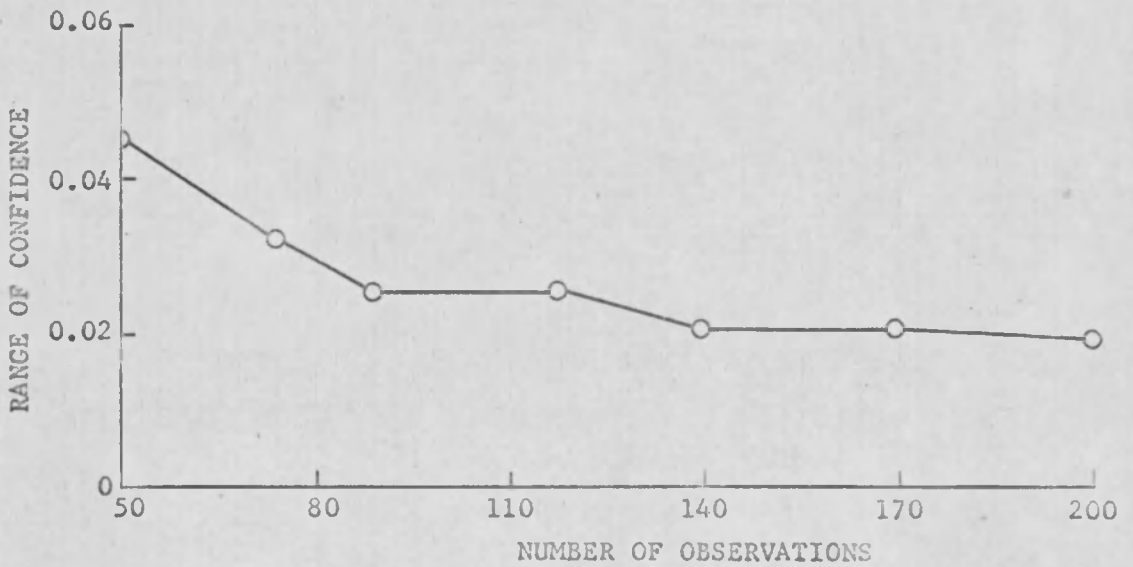
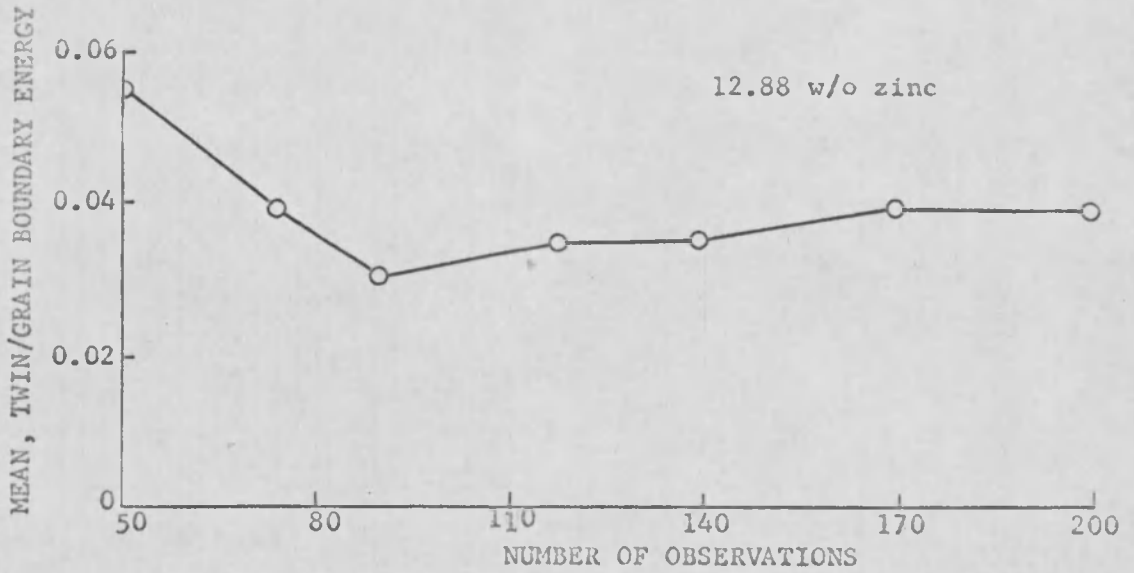


Fig. 5. Variation of mean and range of confidence with number of values of twin/grain boundary energies.

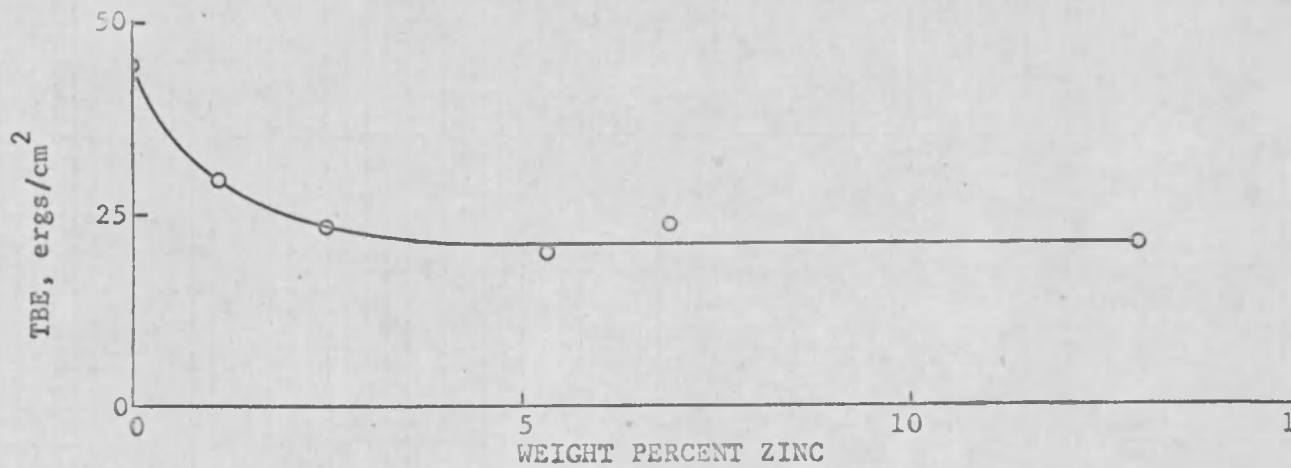
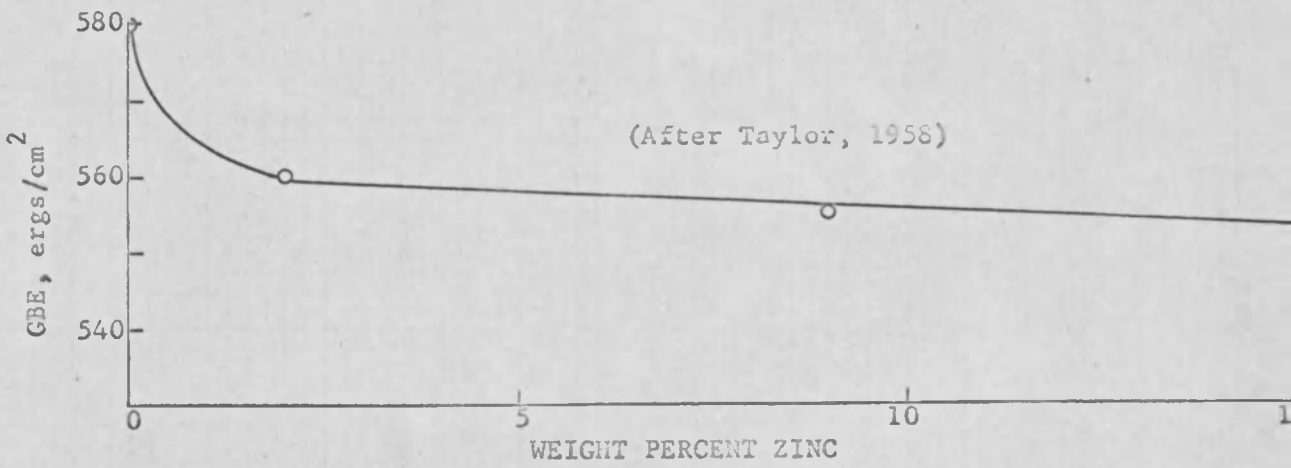
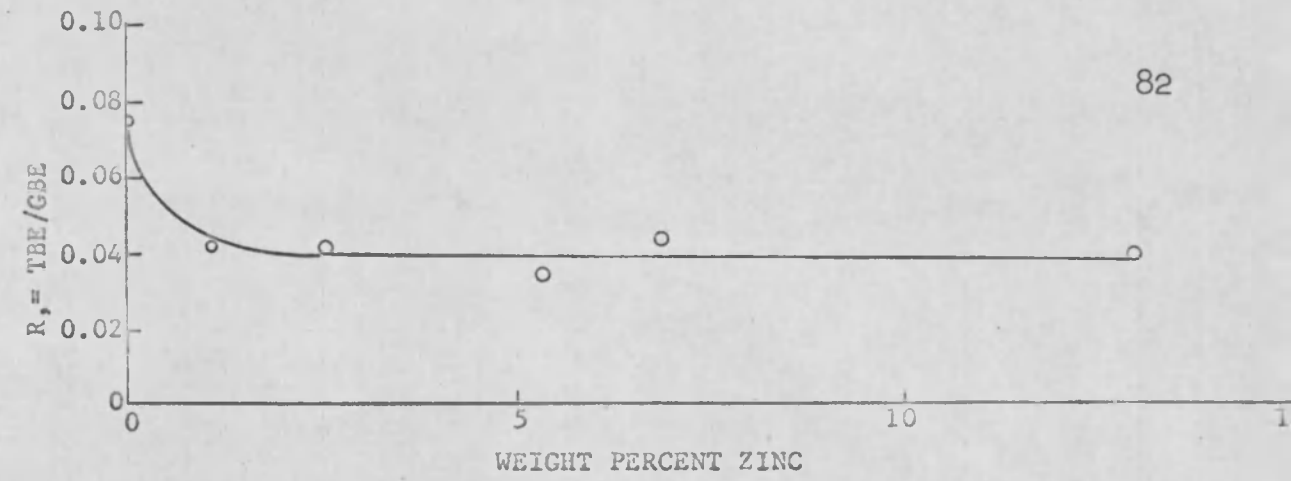


Fig. 6. Twin and Grain boundary energies for Cu-Zn alloys.

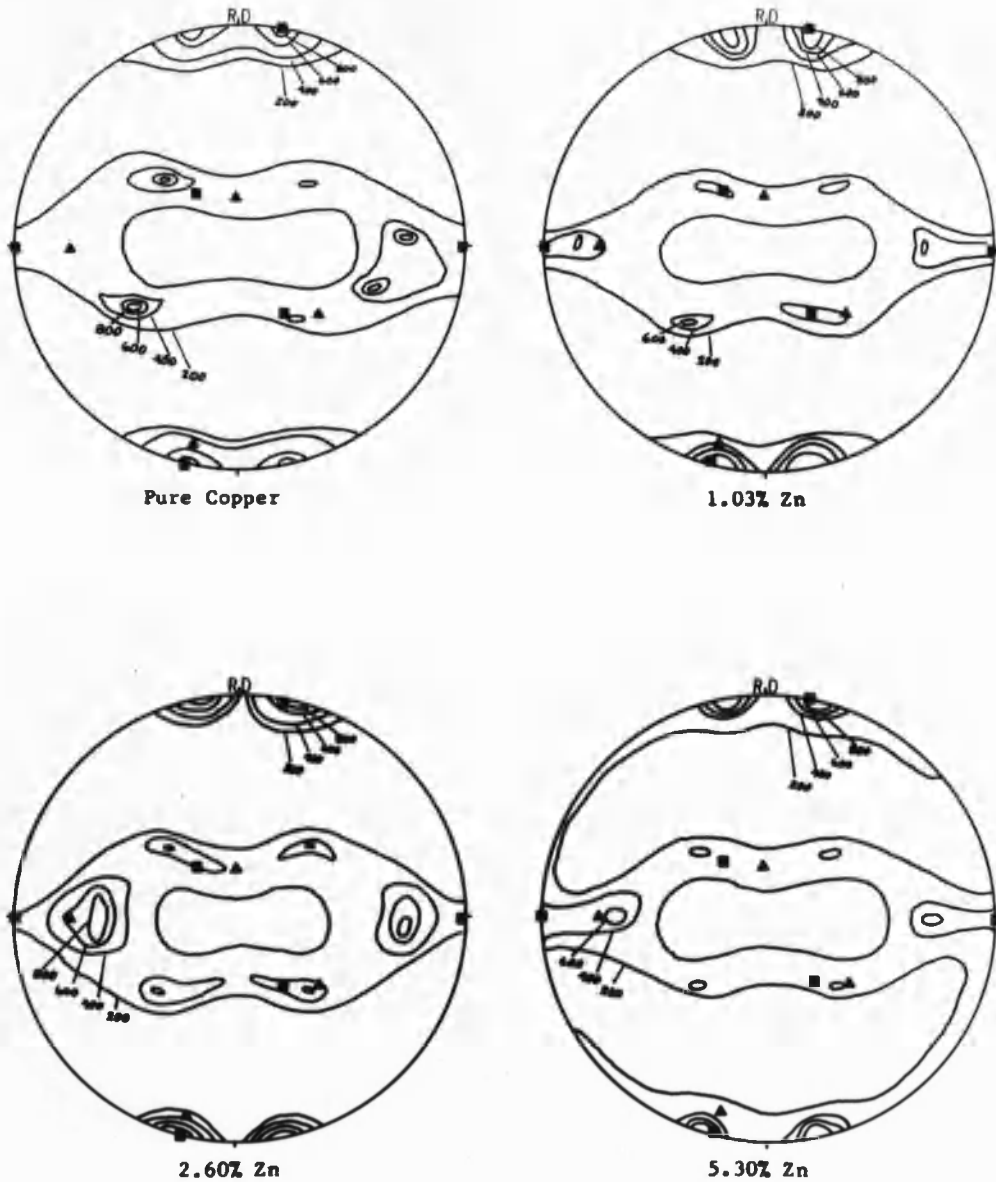


Fig. 7. $\{111\}$ pole figures of high purity copper and brass rolled 98.3%. % zinc in brass as indicated. ■ $\{110\} \langle 112 \rangle$ ▲ $\{531\} \langle 001 \rangle$

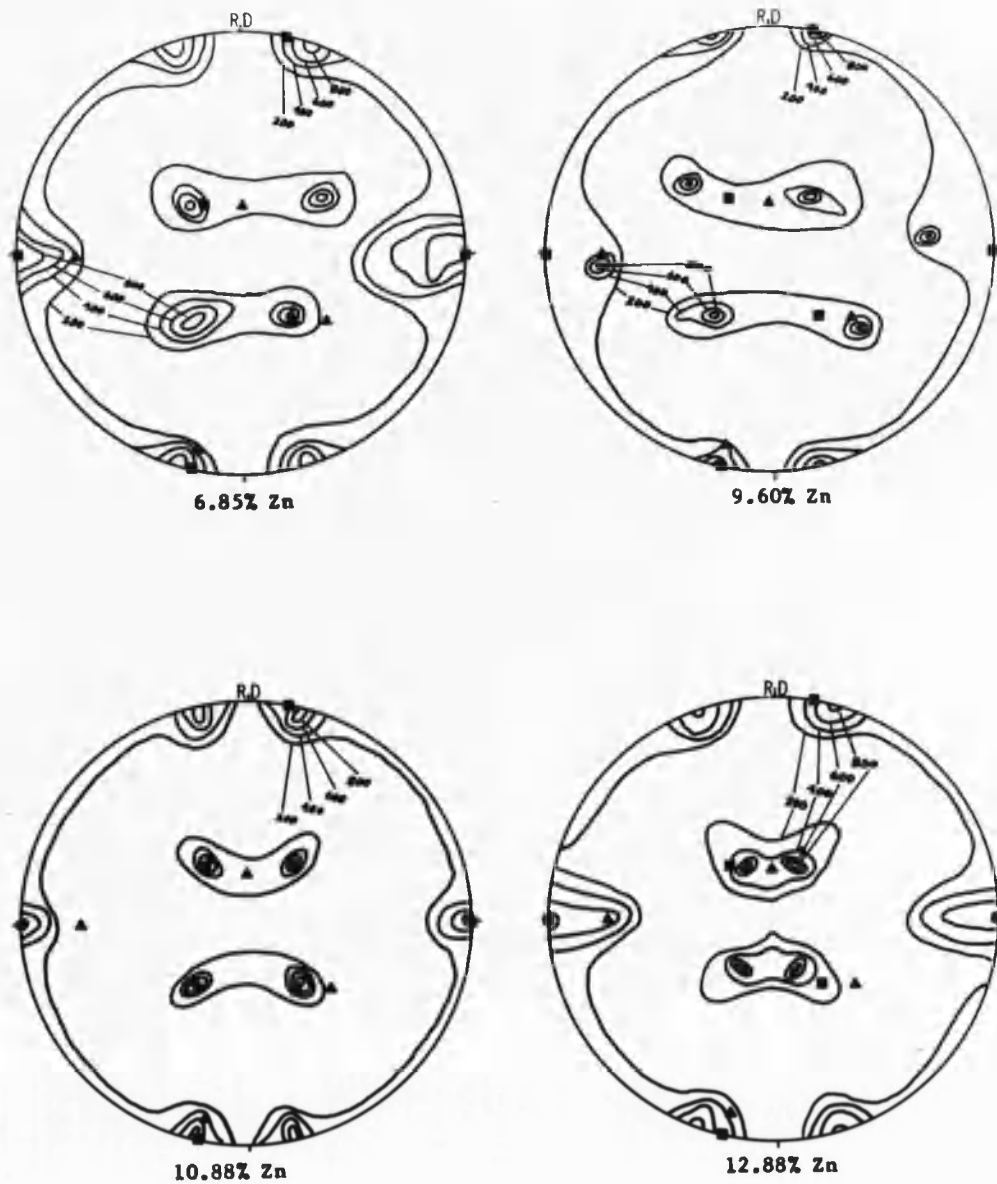
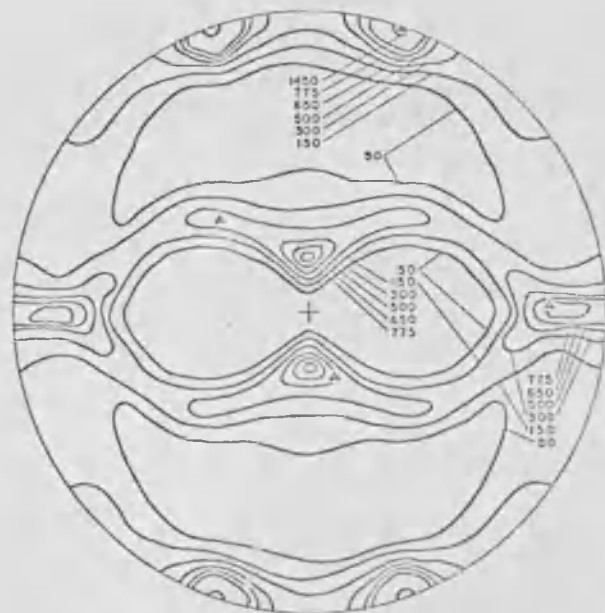
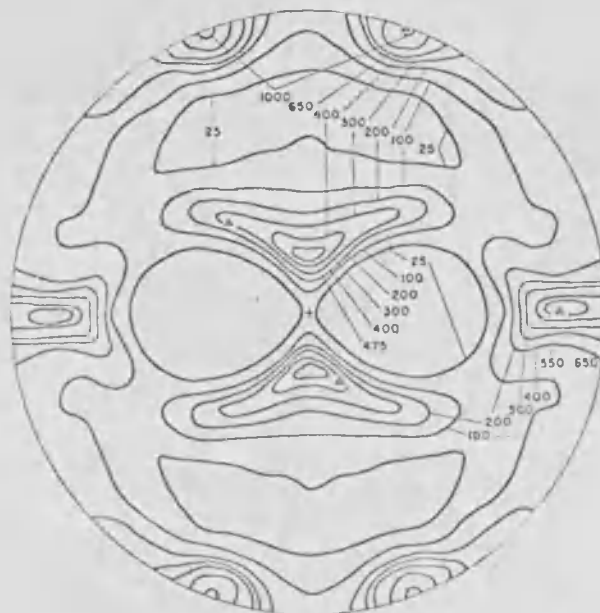


Fig. 8. $\{111\}$ pole figures of high purity brass rolled 98.3% .
 % zinc in brass as indicated. ■ $\{110\} \langle 112 \rangle$ ▲ $\{531\} \langle 001 \rangle$



96.8-3.2 Cu-Zn



93.8-6.2 Cu-Zn



89.7-10.3 Cu-Zn

Fig. 9. $\{111\}$ pole figures of brasses rolled 96%. Weight percent zinc in brasses as indicated. (After Merlini and Beck, 1955.)

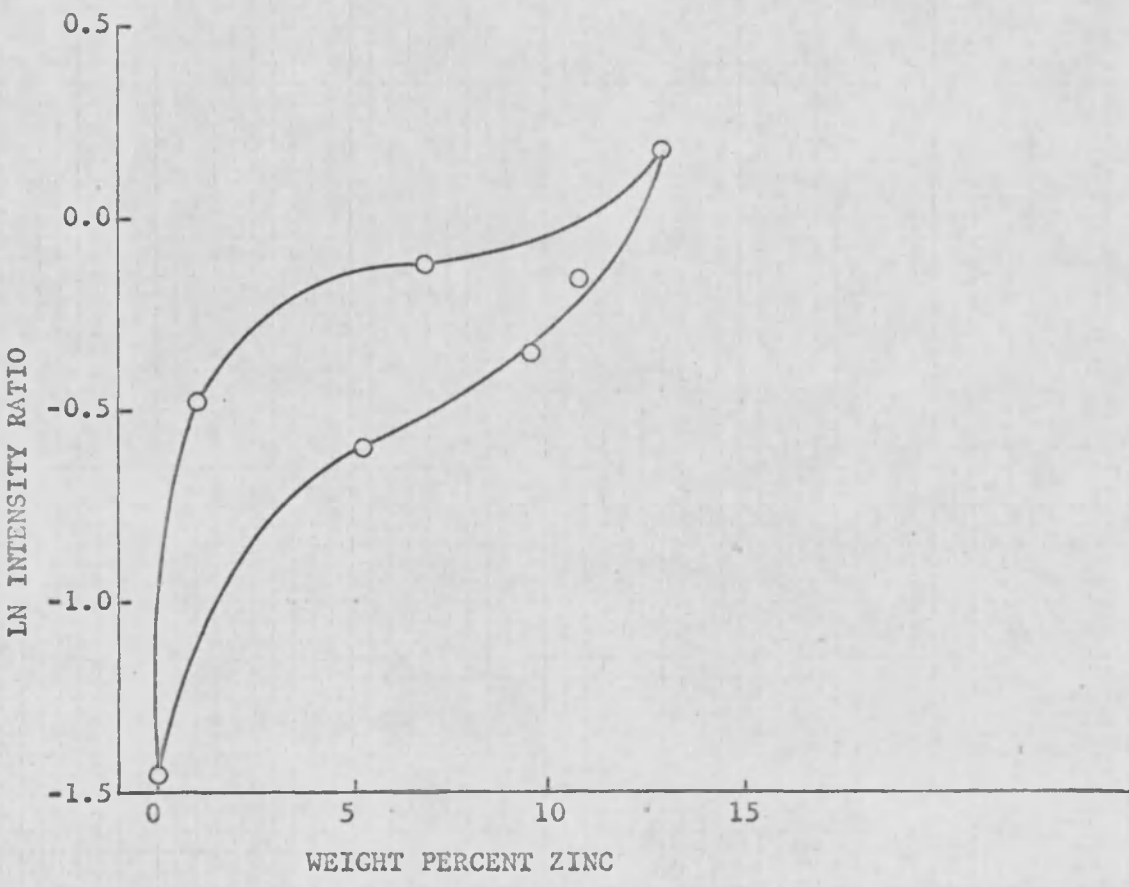
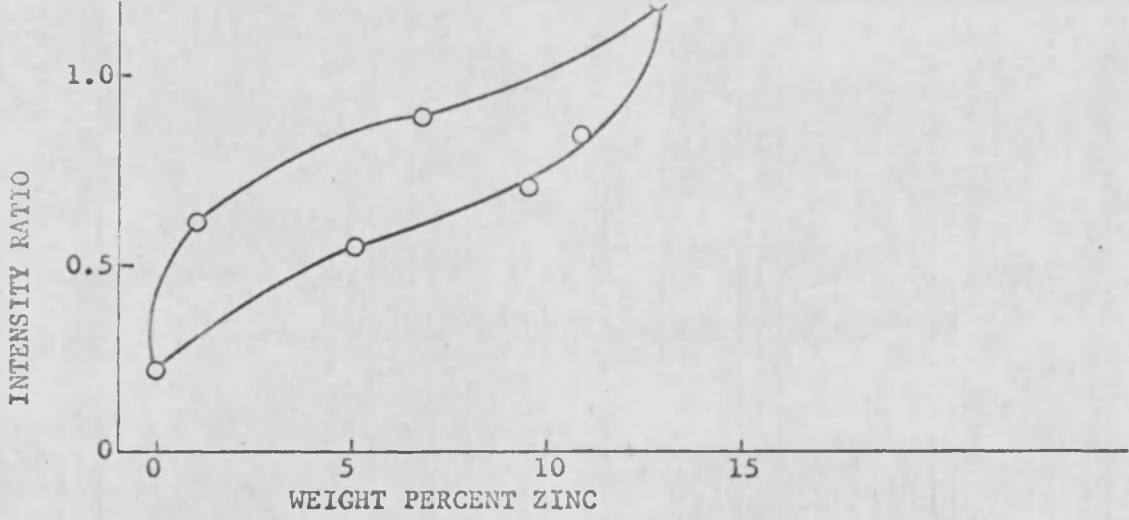


Fig. 10. Variation of texture intensity ratio with weight percent zinc in brass.

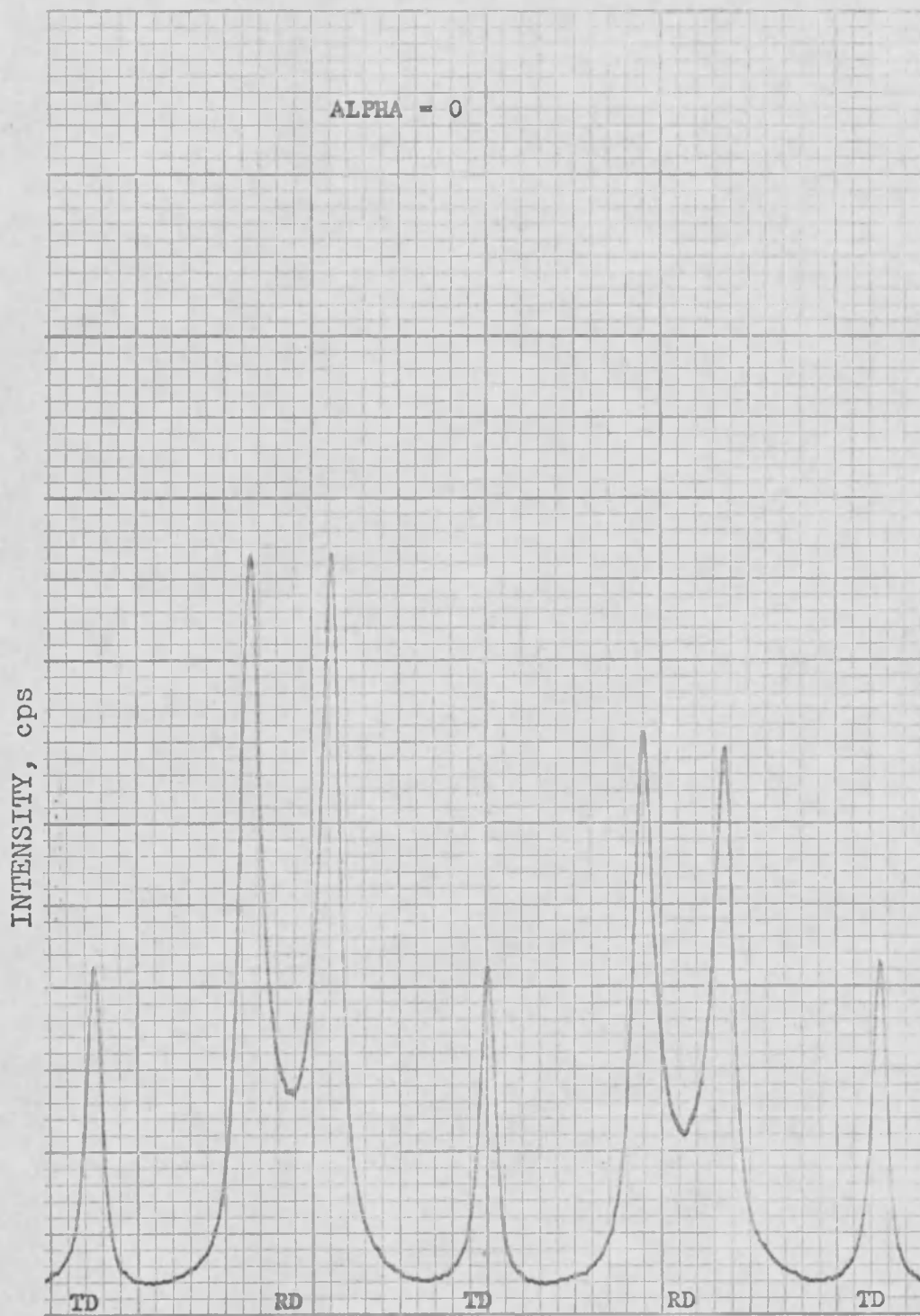


Figure 11. Partial $\{111\}$ pole figure scan of 99.99% copper rolled 76%.



Figure 12. Partial $\{111\}$ pole figure scan of 99.999% copper rolled 98.3%

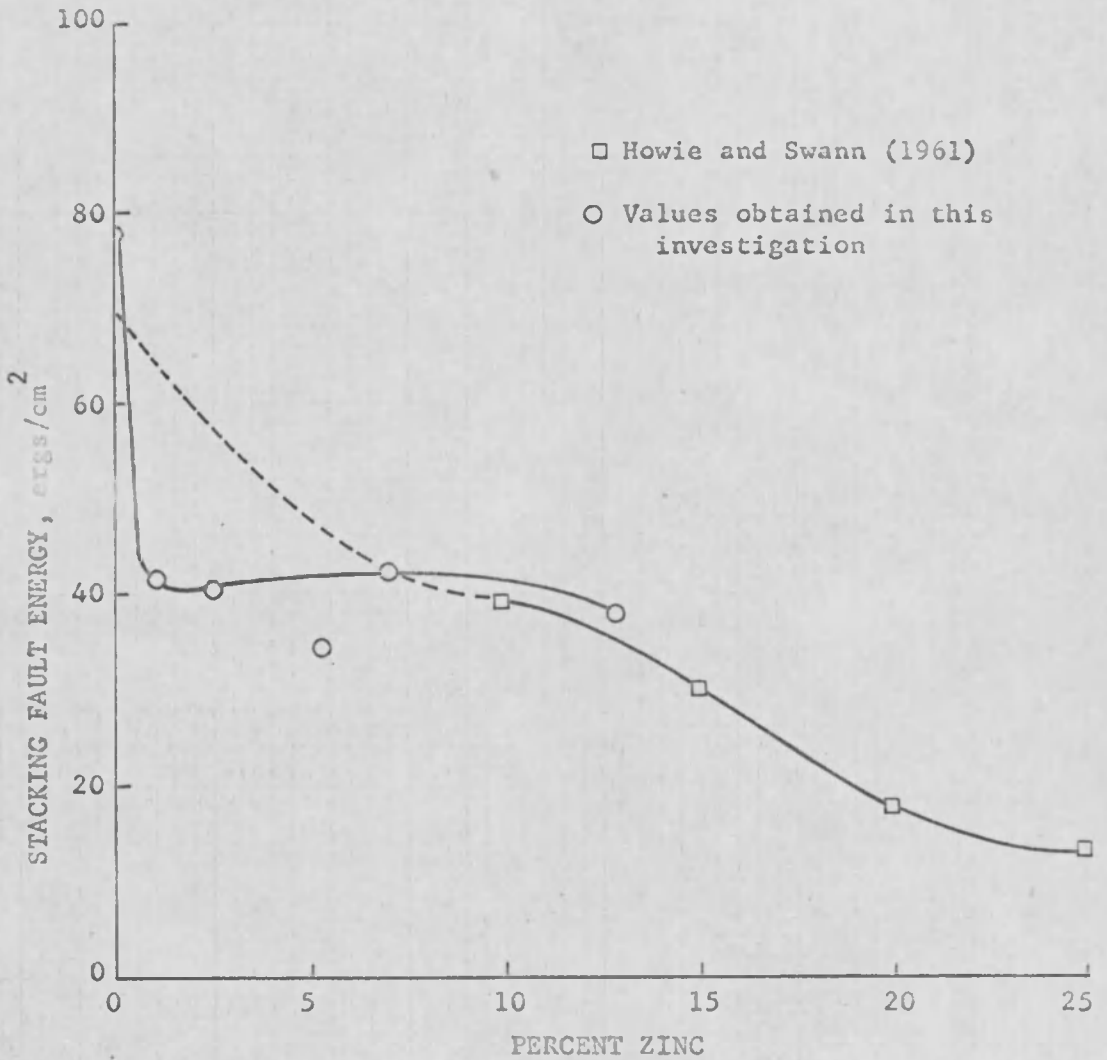


Fig. 13. Apparent stacking fault energies for Cu-Zn alloys. Corrected results of Howie and Swann (1961) are plotted for comparison.

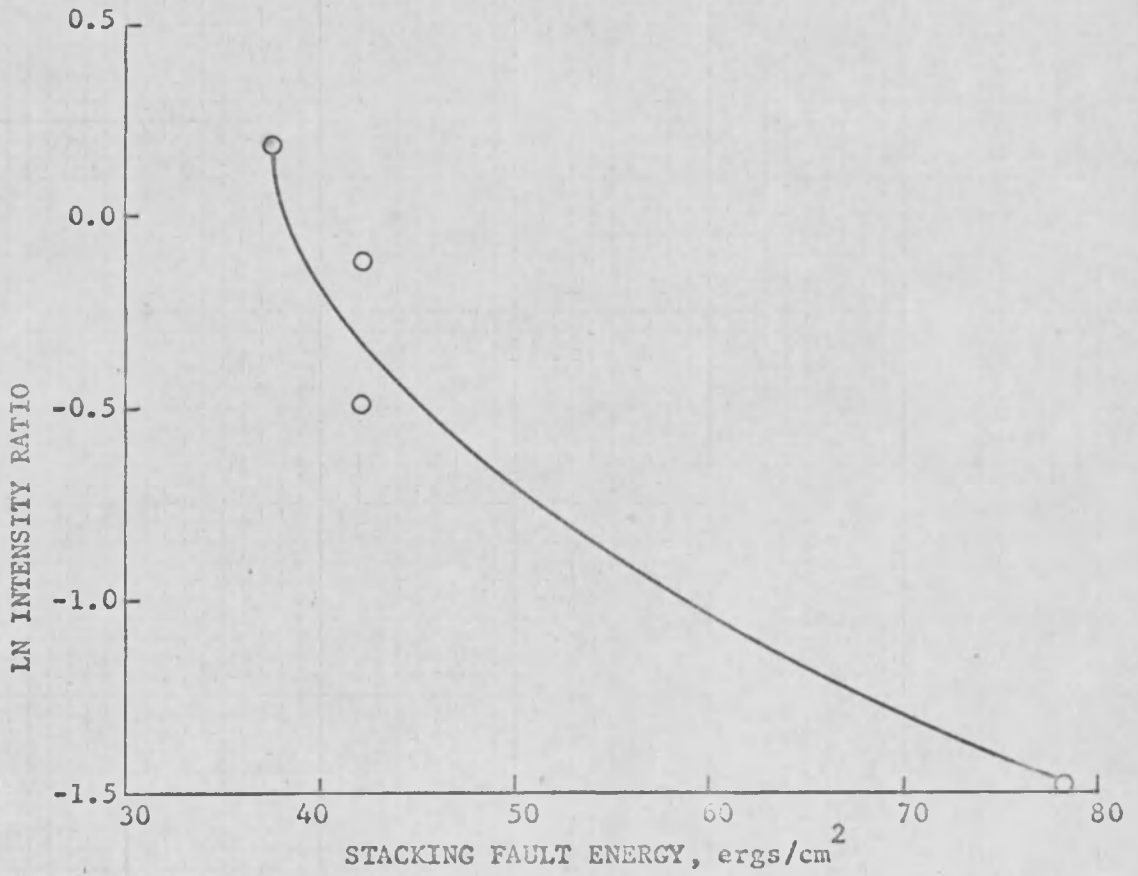
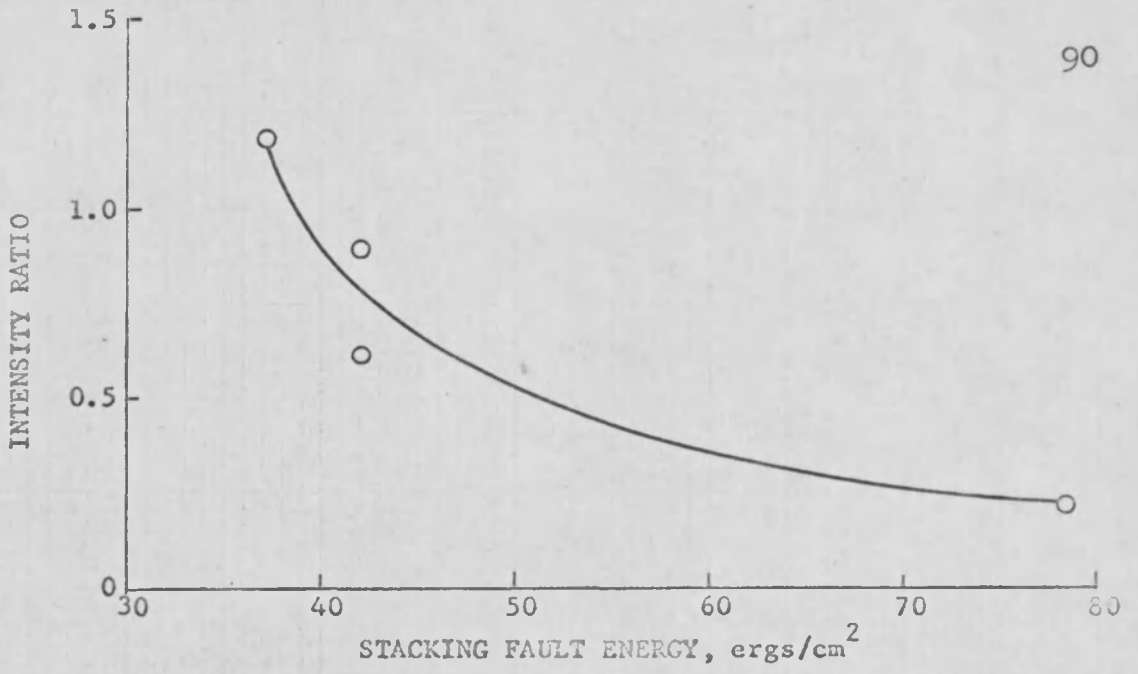


Fig. 14. Variation of texture intensity ratio with stacking fault energy.

APPENDIX A

QUANTITATIVE ANALYSIS OF COPPER-ZINC ALLOYS
BY USE OF THE X-RAY SPECTROMETER

The basis for chemical analysis by x-ray fluorescence is that each element will emit its characteristic lines when bombarded by high energy x-rays. Every element has a characteristic line spectrum. The most intense lines of this spectrum are the K-alpha and the K-beta.

The analysis is carried out with the aid of an x-ray spectrometer by diffracting the radiation from crystallographic planes of known d-spacing in a single crystal. This single crystal, most commonly a LiF crystal, enables the characteristic wavelengths emitted by the specimen to be recorded one at a time.

The analysis may be qualitative or quantitative. In the former method, all that is required is a scan of all possible angles from $\theta = 0$ to $\theta = 90^\circ$. The angles at which intensity peaks occur may then be related to elements which produced the peaks by referring to published tables such as "X-ray Wavelengths for Spectrometer", General Electric Co., 1961. In the latter method, the intensities of the peaks are compared with intensities of lines from a suitable standard.

The steps involved in analyzing alpha-brasses were as follows:

1. Preparation of copper and zinc standard solutions.
2. Determination of optimum setting of x-ray variables.

3. Determination of fluorescent intensity versus percent copper and percent zinc for the standard solutions.
4. Preparation of solutions from ingots.
5. Determination of zinc content of ingots by comparing intensities with the standard curve.

This zinc analysis was made using the GE XRD-5 X-Ray Spectrometer.

The brass standards were prepared by mixing the desired proportions of copper and zinc solutions that were prepared from the pure metals to a concentration of 0.01 gm/cc. For example, a 94-6 Cu-Zn standard solution was prepared by measuring 47 cc of copper solution and adding 3 cc of zinc solution.

The samples were placed in a plastic container with a Mylar window to hold the solutions while they were being irradiated. It was found that it was necessary to use a constant volume such that a flat surface was produced at the Mylar window to obtain reproducible results.

The x-ray variables in this method are (a) KVP, (b) milliamperes, (c) target, (d) analyzing crystal, (e) counter type, (f) 2θ values, (g) counter voltage, and (h) pulse height selector.

The KVP was the maximum voltage recommended for the target used, 50 KVP. The milliamperage was determined as

that current which would enable both copper and zinc intensity peaks to remain within the range of the chart recorder scale regardless of their concentration. The target used was platinum since it was the only one available but proved satisfactory since no platinum peaks appeared near the Cu K-alpha peaks. The analyzing crystal, LiF, was satisfactory because the K-alpha peaks of copper and zinc appeared sharp and intense. The counter voltage was determined by obtaining a counter plateau curve, using the same material as that to be analyzed. The counter voltage was then chosen at about midpoint of the plateau. The 2θ values were determined by obtaining 2θ scans over the range of K-alpha peaks found in tables. These are:

<u>2θ</u>	<u>peak</u>
37.55	Zn K-beta
40.45	Cu K-beta
41.80	Zn K-alpha
45.03	Cu K-alpha

Only the K-alpha peaks were used because these were of the higher intensity. The pulse-height selector filters out reflections which occur near the desired peaks. This was found unnecessary in this case but a voltage window was found desirable to produce sharper peaks.

Below is a listing of all x-ray variables:

KVP	-	50
MA	-	5
Target	-	Pt
Counter	-	Scintillation
Analyzing Crystal	-	LiF
Beam Slit	-	0.010° Soller
Counter Voltage	-	1.3 DC KV

Using the K-alpha peaks for Cu and Zn, the ratio of intensities of the Zn K-alpha to the Cu K-alpha was obtained. This ratio eliminates an internal standard and corrections for day-to-day fluctuations, as well as corrections for any secondary emissions. Intensities were determined by setting the x-ray goniometer to the K-alpha peak and obtaining the counts per second by use of a scaler. The period of counting was 1000 seconds. Values obtained, in counts per second, are plotted in Figure A. The values of the ratios vary by about 0.15 w/o zinc from the curve determined by the method of least squares. Therefore, the overall accuracy should be within this value.

To analyze the ingots of brass, filings from each end of the ingot were obtained and dissolved in a 50% nitric acid solution after which they were diluted to the same concentration as the standards. The analysis then consisted of comparing the Zn K-alpha to Cu K-alpha intensity ratio against the standard curve.

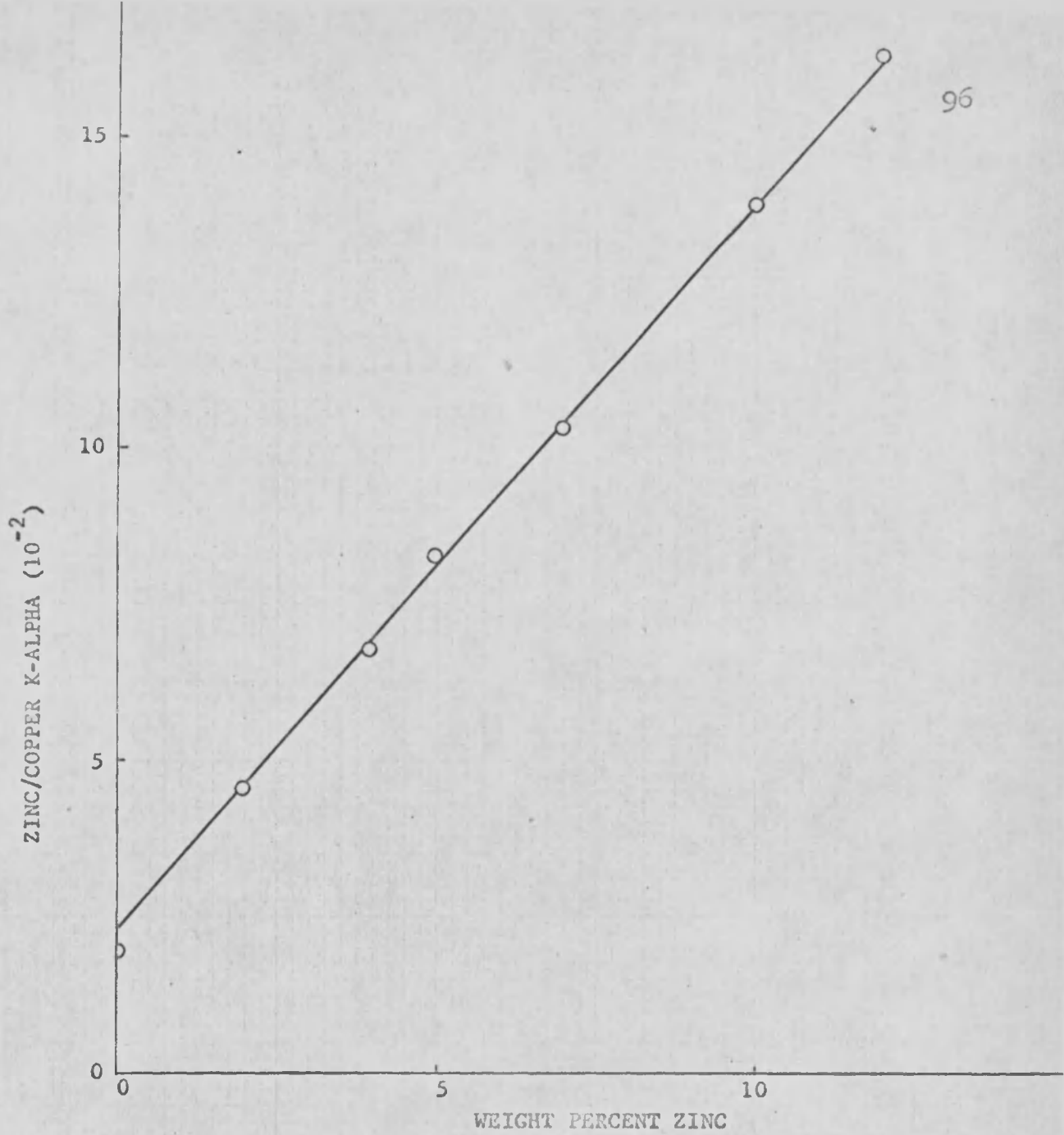


Fig. A. Variation of intensity ratio of zinc K-alpha to copper K-alpha with increasing zinc content.

APPENDIX B

PROCEDURE FOR PLOTTING POLE FIGURES

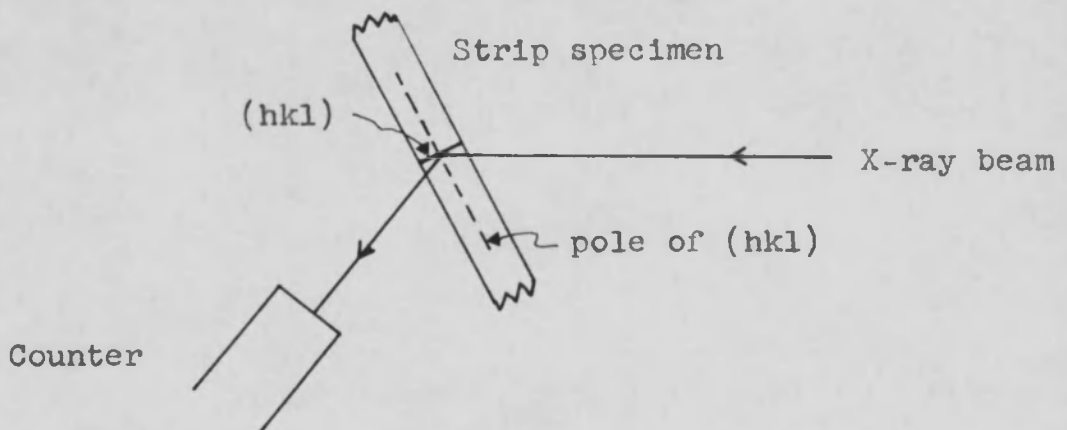
i. INTRODUCTION

When a pinhole x-ray pattern of a polycrystalline metal is obtained, the Debye rings which appear are the result of aggregations of spots formed by reflections of $\{hkl\}$ planes. Each spot corresponds to a particle of powder or a grain which has its $\{hkl\}$ planes oriented so as to make the correct Bragg reflection. In a metal whose grains are oriented randomly, the population of spots around the circumference of the Debye ring is equally distributed resulting in a ring of equal intensity around its circumference. When the metal has its grains preferentially oriented, however, the Debye rings are of nonuniform intensity or even discontinuous around the circumference. The low intensity or missing portions of the rings are due to few or no grains being oriented at those positions for Bragg reflection. The degree and type of preferred orientation or texture, then, may be determined by analysis of the positions and intensities of the Debye arcs.

A diffractometer counter tube counts the diffracted x-ray quanta from a portion of a Debye ring. In order to use this device for determination of preferred orientation of a specimen from a rolled sheet, the specimen must be rotated about an axis perpendicular to its plane (beta angle) so that the entire Debye ring (or arc, in the case of textured specimens) passes through the counter window.

In addition to this rotation, it is necessary to rotate the specimen about an axis in the plane of the specimen (alpha angle), since the texture does not have rotational symmetry about the rolling direction. The latter rotation can be explained further by considering the planes contributing to a given $\{hkl\}$ diffraction.

When the specimen is placed in the pole-figure goniometer for transmission at alpha equals 0° , the specimen plane bisects the angle between the incident and transmitted beam as shown in the sketch on this page. The intensity measured at this alpha angle is due to diffraction from $\{hkl\}$ planes which lie normal to the plane of the vertical specimen holder ring. The pole of the specimen surface lies at the center of the polar net and the poles of the $\{hkl\}$ planes, therefore, lie on the periphery of the net. The polar net corresponds to the face of the specimen as viewed from the counter.



If the specimen is rotated about the diffractometer axis from its zero position by 5° alpha, the intensity measured is the result of diffraction from $\{hkl\}$ planes located 5° from the normal to the plane of the vertical ring. This corresponds to a rotation of the $\{hkl\}$ poles also of 5° along a meridian. The pole of this rotated plane, then, lies at 5° from the periphery towards the center of the net.

When a scan of a textured specimen is made through several alpha angles as described above, the data can be used to plot a stereographic view of the distribution of $\{hkl\}$ planes for the specimen. From these pole-figure plots, information such as type and degree of preferred orientation, deviation from ideal textures, comparison of mode of deformation between metals and alloys, texture transitions, etc. can be obtained.

Since the intensities obtained in pole-figure scans are dependent upon such factors as machine characteristics and specific techniques used, it is desirable and common practice to use intensities based on a sample of the same material of random orientation. This tends to afford reproducible results independent of different machines and techniques.

A detailed discussion of the various specific procedures involved in obtaining a pole figure is offered below and arranged according to the following general topics:

- A. Preparation of Random Sample
- B. Determination and Setting of Optimum Machine
Operating Conditions
- C. Obtaining Data from Random Sample
- D. Preparation of Textured Sample
- E. Obtaining Data from Textured Sample
- F. Analysis and Plotting of Data on Polar Net

The procedures described here are based on the preparation of pole figures using a General Electric XRD-5 X-ray Diffraction Unit equipped with a General Electric Automatic Integrating Pole-Figure Goniometer.

ii. POLE-FIGURE PREPARATION PROCEDURE

A. Preparation of Random Sample

There are several ways of preparing a randomly oriented sample. Among these are spraying of the powder mixed with Glyptal varnish (Geisler, 1953) or using gravity settling of powder through molten paraffin followed by firing of the paraffin-impregnated powder (Newkirk and Bruce, 1957). The following method adopted in this laboratory has also proved to be satisfactory.

A.1. Machine a piston-cylinder die with the inside diameter of the cylinder equal to the diameter of the specimen holder on the pole-figure goniometer. Actually, a somewhat larger diameter would be more satisfactory to eliminate edge etch effects on the finished specimen.

A.2. With the piston in the cylinder, place enough powder to obtain a thick compact (about 1/8 in. or less of loose powder). A thinner compact will result in a textured sample. Using a heavy-duty laboratory press, prepare the compact. Sinter the compact, then grind the specimen to the standard thickness. The specimens should be reduced as far as possible mechanically and then etched to the desired thickness. The thickness should be enough to provide essentially complete absorption of the primary beam for the reflection method but not much thicker than about 0.010 in. It is possible to use the same specimen for both transmission and reflection if the thickness is less than about $2/\mu$, where μ is the linear absorption coefficient (ASTM Std. E81-54T, Pt. 3, 1961).

B. Determination and Setting of Optimum Machine Operating Conditions

Target -- The choice here is dependent upon the absorption of the test material.

KVP-MA -- This is chosen to obtain maximum intensity without exceeding the x-ray tube limitations.

Beam Slit -- Slits are chosen as a compromise between intensity and resolution. The wider the slit, the higher the intensity at the expense of resolution. The beam width at the beam slit should be sufficiently narrow to prevent the beam from striking the specimen holder at

any alpha angle. This slit should also be wide enough to provide adequate intensity for pole-figure traces. It may be necessary to mask off the beam at this slit to prevent the beam from striking the top and bottom of the specimen holder as it oscillates.

Pole-Figure Goniometer -- This device automatically provides the necessary rotations as explained previously.

Beta rotation -- is rotation of the specimen about an axis normal to the specimen surface in angular increments of 16 minutes of arc. This rotation is at the rate of one revolution in 45 minutes, and is clockwise as viewed from the counter.

Alpha rotation -- consists of rotation of the specimen holder in discrete 5° steps about the goniometer's vertical theta axis. The rotation is clockwise as viewed from above.

Operation:

1. Determine the alpha ranges to be used in transmission and reflection. In transmission, alpha equals zero when the specimen holder pointer is at zero. The alpha range is limited by beam interference from the specimen holder. The available ranges depend also on the 2θ angle being used. For greater range in the overlap region, it is advisable to use a higher order plane in reflection. For

aluminum, using (111) for transmission and (333) in reflection, the following ranges were possible: transmission -- 0° to 55° alpha, reflection -- 90° to 55° alpha.

2. Determine the number of quadrants necessary to investigate in order to obtain the complete pole figure. Most types of deformation produce a 180° symmetry and in many cases a 90° symmetry; that is, one quadrant is sufficient to describe the whole pole figure, in the latter case. In some cases, however, it may be desirable to use a full 360° of beta rotation at each alpha angle. When this is determined, set the beta range on the goniometer controller.

3. Set beta at 0° and insert specimen into the specimen holder with the rolling direction vertical. This results in having the rolling direction at beta = 90° on the polar net since the portion of the Debye arc at the counter lies at a right angle to the rolling direction.

4. Set alpha at 0° for transmission or at 90° for reflection.

5. Press ready button until green light turns on, on the controller panel, then press once more. In the case where 90° beta increments are used, it is unnecessary to use the ready button.

6. Begin pole-figure trace by simultaneously starting recorder chart and pole-figure goniometer.

Detector Slit -- Since the alpha rotation alters the geometry of the focusing circle, the detector slit does not increase the resolution by very much at alpha angles greater than zero. The detector slit also cuts down the width of the peak entering the counter. For the pole-figure preparation procedure described here this is not an important factor. However, when calculating intensities for alpha angles other than at zero degrees, as suggested by Decker, Asp, and Harker (1948), it is necessary to use integrated intensities and, therefore, the whole width of the 2θ peak must enter the counter.

Filter -- Use the recommended filter for the target being employed. In incident beam since the highest ratio of I_{hkl} to $I_{background}$ is given in this arrangement (Newkirk and Bruce, 1957).

Chart Speed -- The chart speed to use is almost an arbitrary choice, but the best compromise between using a large amount of paper and having too much peak convergence seems to be at 12 in./hr.

Chart Scale -- The log scale is most commonly used. The use of this scale necessitates a log ruler to be prepared by reading several intensity counts along the scale after calibrating the scale to read 10,000 counts at full scale. Note: the log scale on the chart is not a base "e" or base "10" but is an "electronic" log scale. The linear scale can also be used when the highest peak

intensity lies within the range of the scale used. This scale is sometimes more convenient than the log scale because the intensities are easy to read, the scale is simple to calibrate, and the low intensity insignificant peaks are not so prominent.

X-Ray Unit Stabilization -- When the unit (power and tube) is cold, a markedly higher intensity will be recorded. As the unit warms up, the intensity drops off in an exponential manner and levels off after about 40 minutes of operation. The line voltage and tube, then, should be run approximately 45 minutes before performing any operation which involves intensity measurements. If a standard intensity sample is available, it is more convenient and accurate to use this than to wait for a specific time.

Specific Conditions -- The following conditions were used for obtaining a pole figure of aluminum:

Transmission:

KVP 50 MA SPECIMEN Al COUNTER Proportional
 SPG-6 RADIATION CuK FILTER Ni (in filter slot)
 BEAM SLIT 3° MR with mask ALPHA RANGE 0° to 55°
 SOLLER SLIT MR DETECTOR SLIT none CHART
 SPEED 12"/hr. BETA RANGE 0° to 360° 2 θ
38.6° (111)

Reflection:

The same conditions were used as above except for the alpha range which in this case was 90° to 55° , a change in the filter placement to a position in the diffracted beam, and a different 2θ , in this case 162.5° for the (333) reflection.

C. Obtaining Data from Random Sample

If this sample is to be used subsequently as a standard intensity sample, it is desirable to allow a longer warm-up time for line and tube than prescribed above.

C.1. Randomness -- The randomness may be checked either by a pole-figure trace or by a pinhole x-ray photograph. The former is the more exact method.

C.2. Absorption factor, μt -- The procedure to be used is as follows:

a. Using the identical 2θ and slit and filter arrangements to be used for pole-figure scans, set a diffraction specimen, preferably of the same material, on the specimen holder. Determine the counts/sec. on the scaler. This figure is I_0 .

b. Set the sample in front of the counter window and obtain the counts/sec. This figure is I .

c. From several readings, or longer counting time, determine the mean μt for the sample by the relation:

$$I = I_0 e^{-\mu t}.$$

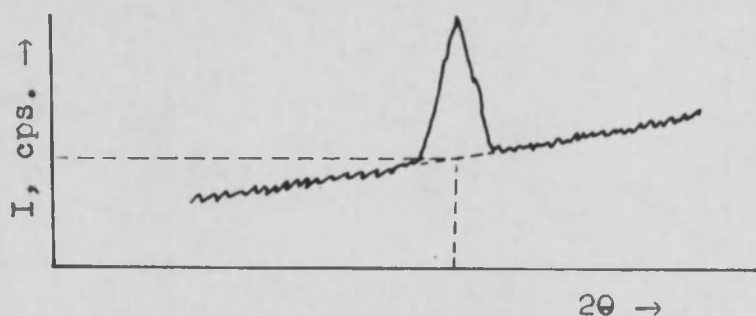
Note: The μt will not be the same for different 2θ values due probably to phenomena such as secondary emission.

C.3. Background Intensities -- The purpose of obtaining these background intensity measurements is ultimately to plot and report intensities above background and thereby produce reproducible pole figures which are independent of machine and operating conditions.

For the chosen 2θ angles in transmission and reflection, the background is determined for all alpha angles to be used. When no overlapping peaks are present at the chosen 2θ , these backgrounds may be determined by either of the following methods:

a. Obtain a slow rate 2θ scan to include portions on each side of the peak and note the trend of the background intensities. Use the interpolated value as background intensity.

Example:



b. Using the value of background for only $\alpha = 0$, calculate the rest of the alpha backgrounds by the intensity correction, I_0/I_μ , which can be obtained from the data in step F below.

In the case where overlapping peaks occur in the near vicinity of the 2θ peaks, Acucena and VanKuren (1958) outline a background intensity determination method.

If the background intensity from the random sample is above the lowest trace given by the textured sample, the random sample is not a true random representation.

C.4. Lattice Parameter -- A comparatively large difference in lattice parameter or, more specifically, a large difference in line position of a textured sample as compared with the random sample, will cause the intensity of the textured sample to be too low at the 2θ angle used for the random sample. It is convenient, therefore, to be able to determine beforehand if a pole figure of a certain alloy of the random sample material may be prepared using the same random sample. A knowledge of the lattice parameter of the random sample and the alloy in question accomplishes this purpose.

Even when the lattice parameter does not change significantly, however, slight apparent peak shifts can occur with different alpha angles. The difference in intensity on the pole-figure scan can be as high as a factor of two. If this "peak shift" is not equal for

different conditions of specimen treatment or alloying, then this can affect the interpretation of a series of pole figures.

D. Preparation of Textured Sample

The preparation of the textured sample depends, of course, on the starting and ultimate material conditions desired. An example will be outlined herein, in which a cast aluminum ingot was reduced, rolled, and prepared as a pole-figure specimen.

The specimen from the ingot was first alternately compressed to a predetermined reduction and annealed until it could be accommodated by the available rolling mill.

The reductions were determined by the relation:

$$\% R = 1 - (F/I)^{(1/n)},$$

where $\% R$ = percent reduction

F = final thickness

I = initial thickness

n = number of passes.

The reduction per pass, or compression operation, was determined by the work hardening of the material used, as well as by the capacity of the press being used.

The specimen was checked, at this stage, for texture by a pinhole pattern or pole-figure trace. Since the specimen was to be rolled less than 90%, it was required that it

be all or nearly texture free. If a specimen is to be rolled greater than 90%, the compression texture will probably disappear. The specimen was then rolled to the desired reduction and a section was punched out, using the powder compact die. The punched-out specimen was then ground and etched to the absorption factor of the random sample.

Alternate methods of reducing the specimen are by chemical and electrolytic techniques. In the latter, however, reaction products may form on the surface and consequently may cause spurious peaks to appear in the pole-figure scans. It is probably possible to etch this surface layer off. In both methods there is danger of losing a constituent, in the case of alloys, due to preferential action on the specimen.

E. Obtaining Data From Textured Sample

E.1. Lattice Parameter -- The lattice parameter is determined for the purpose previously mentioned in C.4.

E.2. Absorption Factor, μt -- The absorption factor for the textured specimen is determined in a similar manner to the random sample. In addition, it may be necessary to obtain I readings at short beta intervals due to absorption differences. Newkirk and Bruce (1957) report that the apparent μt of a textured specimen (of Fe) was found to vary as much as 45% with beta orientation. In high-purity Al, 7178-T6, and Cu, the μt did not vary

significantly with beta orientation. In the case where the μt varies with beta, a weighted average of the μt values should be used.

E.3. Background Intensities -- These are determined in a manner similar to that described for the random sample.

E.4. Pole-Figure Traces -- The following steps may be taken to obtain the pole-figure traces:

a. Set alpha at zero and allow beta to rotate through 90° , 180° , or 360° on a certain 2θ .

b. Correlate the motion of the recorder chart with the beta rotation, and mark the prominent directions in the specimen (such as the rolling direction) on the chart to be used as the origin for measuring angles.

F. Analysis and Plotting of Data on Polar Net

F.1. Random Sample Chart Preparation -- Details of the procedures for transmission and reflection are given below.

a. Transmission:

A convenient form of tabulation of data is the one on the following page.

I	II	III	IV	V	VI	VII	VIII	IX
Alpha	Counts	Seconds	CPS	Random BG	Random I Above BG	Textured BG	1X	2X

Col. I : Use alpha range as determined in step B.

Col. II, III, IV : The intensity at each alpha angle is determined by counting continuously through the beta range used. This is accomplished by setting the scaler on "Manual" and using the "Stop" lever when the indexing occurs. Using the time recorded on the scaler, the average cps value is determined. Another method is to draw an iso-intensity line on the recorder chart which best averages the intensity trace.

Col. V : These are determined as outlined in step C.3. above.

Col. VI : Subtract value in Col. V from value in Col. IV.

Col. VII : These are determined as outlined in C.3. above.

Col. VIII : Add value in Col. VI to value in Col. VII.

Col. IX : Twice the value in Col. VI plus value in Col. VII. Other multiplicities of random sample intensity are used which are estimated to intersect peaks on the pole figure trace. Each multiplicity should be marked with a different color which will aid in identification when

plotting the pole figure.

I at 1X = Random I Above BG plus Textured BG.

I at 2X = 2 (Random I Above BG) plus Textured
BG.

Note that I at 2X is not equal to 2 (I at 1X).

b. Reflection:

A convenient form of tabulation of data
in this case is given below.

I	II	III	IV	V	VI	VII
Alpha	Counts	Seconds	CPS	Random BG	Random I Above BG	Corr. for Overlap
VIII	IX					
Text.	1X					

The columns in reflection are similar to those in transmission with the exception of Col. VII. The use of equicolor multiplicities for different alpha angles in transmission, as well as in reflection, provides the necessary correction for increase in absorption and diffracting volume with alpha angle. In effect, in the case of transmission, all alpha angle intensities are increased to the value of the intensity at alpha equals zero. Similarly, in reflection all alpha angle intensities are decreased to the value of the intensity at alpha equals 90° . It is then desirable to conciliate the intensities in reflection to those in transmission.

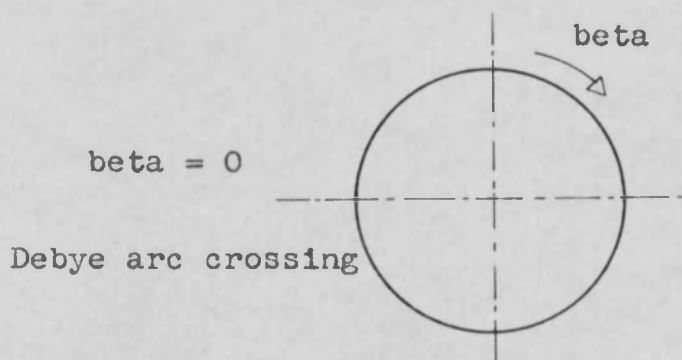
To accomplish this conciliation two methods are suggested: (a) the use of a correction factor on reflected region intensities $I_{\alpha=0^\circ} / I_{\alpha=90^\circ}$; or (b) preparation of samples such that these intensities will be equal. In the former method, even after applying the correction factor, the transmission and reflection intensities may not coincide. In the latter method it is necessary to thin the specimen until the transmitted intensity equals the reflected intensity. This may not be possible for all metals.

F.2. Plotting the Pole Figure --

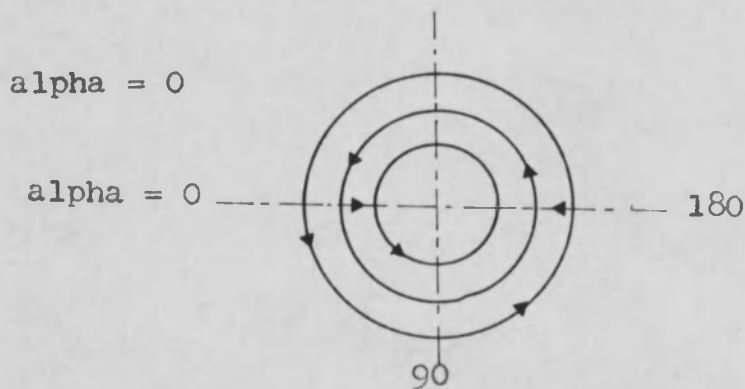
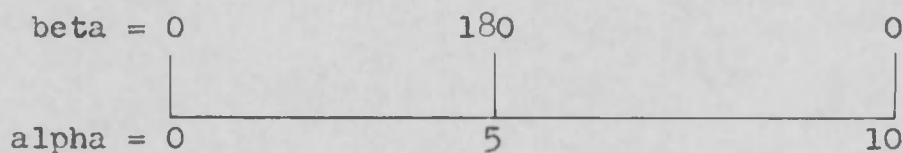
a. Make a calibrated rule for beta degrees such that the thickness of a peak at a certain intensity horizontal line may be measured in beta degrees.

b. The beta angles at which each trace crosses an intensity level are measured with this rule, and a point at the corresponding alpha and beta coordinates is plotted on a polar stereographic chart in a color characteristic of the intensity level. The polar chart has beta degree graduations on its circumference and increasing alpha degree graduations in receding concentric circles. It is advisable to plot all arcs of one peak for all the alpha angles and to join these arcs into one contour before plotting other peaks to prevent confusion in drawing the contours. Illustrations of these measurements, as well as the final contour lines are shown on pages 148-151 in "Modern Research Techniques", A.S.M., 1953.

c. Sequence of Plotting: In transmission, with alpha set at zero, the beta rotation is clockwise as viewed from the counter. This causes the Debye arcs to pass across the counter window in a counterclockwise sequence from beta equals zero, as indicated below.



For 180° symmetry, the pole figure is plotted in the following sequence:



In reflection, for 180° symmetry, the pole figure is plotted in the sequence shown below:

